12-14-2014

Use of Thermally Grown Oxide Stress Measurements to Predict Remaining Life of Thermal Barrier Coatings under Realistic Turbine Engine Conditions

Nirav V. Patel
nirav625@gmail.com

Use of Thermally Grown Oxide Stress Measurements to Predict Remaining Life of Thermal Barrier Coatings under Realistic Turbine Engine Conditions

Nirav Vijay Patel

B.S., University of Connecticut, 2013

A Thesis

Submitted in Partial Fulfillment of the

Requirements for the Degree of

Master of Science

at the

University of Connecticut

2014

APPROVAL PAGE

Master of Science Thesis

Use of Thermally Grown Oxide Stress Measurements to Predict Remaining Life of Thermal Barrier Coatings under Realistic Turbine Engine Conditions

Presented by:

Nirav Vijay Patel, B.S.

Major Advisor_____
Eric H. Jordan

Associate Advisor_____
Michael W. Renfro

Associate Advisor_____
Maurice Gell

University of Connecticut

2014

Acknowledgements

I would like to thank my advisors, Dr. Eric Jordan, Dr. Michael Renfro, and Dr. Maurice Gell for the guidance, encouragement, and help they have provided over the past two years. Their advice and instruction truly helped to bring this work to its current state. In addition, I am forever grateful to the University of Connecticut. From the beginning of my time as an undergraduate, the university has always provided me opportunities to grow as an adult, and has shaped the person I am today.

I would like to extend my sincerest thanks to my lab-mates, Martin, Johnny, Rishi, Alan, and Chen for their assistance and teaching me the various testing and preparation procedures used in this study.

My thanks go out to Roger Ristau and Lichun Zhang for training and assisting me on the scanning electron microscope, Gary Lavigne for his advice concerning the Ramascope, and to Peter Glaude for coming up with novel techniques to machine and fabricate the various designs I presented.

Finally, I would like to thank my family, especially my mom and dad who have always been supportive and loving throughout the years.

Table of Contents

1. Introduction 1
1.1 Thermal Barrier Coatings Review 1
1.1.1 Ceramic Top Coat 2
1.1.2 Bond Coat and Thermally Grown Oxide 3
1.2 Photoluminescence Piezospectroscopy (PLPS) 4
1.3 Current Life Prediction Models 5
2. Experimental Setup 7
2.1 TBC Specimens 7
2.2 Furnace Cycling Tests 8
2.2.1 Multiple Amplitude Testing 9
2.3 Photoluminescence Piezospectroscopy Procedure 9
2.4 Sample Preparation for Microscopy 10
2.4.1 Sectioning, Mounting and Grinding 10
2.4.2 Scanning Electron Microscopy 11
3. Experimental Results 15
3.1 Type I TBC Spallation Lives in Constant Cycles 15
3.2 Type I TBC Spallation Lives in Multiple Amplitude Tests 15
3.3 Type I TBC TGO Stress as a Function of Life Fraction for Multiple History Tests 16
3.4 Type II TBC Spallation Lives in Constant Cycles 16
3.5 Type II TBC Spallation Lives in Multiple Temperature Tests 17
3.6 Type II TBC TGO Stress as a Function of Life Fraction for Multiple History Tests 17
3.7 Type A TBC Spallation Lives 17
3.8 Type A TGO Stress as a Function of Life Fraction 18
3.9 Type B TBC Spallation Lives 18
3.10 Type B TGO Stress as a Function of Life Fraction 18
3.11 Scanning Electron Microscopy of Type A Samples 19
3.11.1 SEM of As-Received Type A Sample 19
3.11.2 SEM of Type A Sample A1 (220 cyclic life) 19
3.11.3 SEM of Type A Sample A3 (160 cyclic life) 20
3.12 Scanning Electron Microscopy of Type B Samples 21

3.12.1 SEM of As-Received Type B Sample 21
3.12.2 SEM of Type B Sample B2 (520 cyclic life) 21
3.12.3 SEM of Type B Sample B5 (80 cyclic life) 22
4. Discussion 33
4.1 Linear Damage Rule for Type I and Type II TBC's 33
4.2 Remaining Life Estimates from Stress vs Life Fraction Curves for Type I and II TBC's 34
4.3 Premature Failure of Type A Samples 37
4.3.1 SEM Microscopy of Type A Samples 37
4.3.2 X-Ray Diffraction of Type A Samples 39
4.4 Premature Failure of Type B Samples 39
4.4.1 SEM Microscopy of Type B Samples 39
4.4.2 X-Ray Diffraction of Type B Samples 41
5. Conclusion 54
References 57
Appendix 60

List of Figures and Tables

Figure 1.1: Thermal barrier coating system [25] 6
Figure 2.1: Type I and Type II TBC coupon sample geometry [25] 12
Figure 2.2: Furnace cycle temperature profile for 1-hour cyclic tests [25] 12
Figure 2.3: Furnace cycle temperature profile for 24-hour cyclic tests [25] 12
Figure 2.4: Schematic for the PLPS setup used on Type A and Type B samples [23]..... 13
Figure 2.5: Cracking in the bond coat during polishing of Type A and B TBCs 13
Figure 3.1: Multiple temperature TGO stress versus life fraction for Type I TBC samples 24
Figure 3.2: Multiple hold time TGO Stress versus life fraction for Type I TBC samples 25
Figure 3.3: Multiple temperature TGO Stress versus life fraction for Type II TBC samples 26
Figure 3.4: TGO Stress versus life fraction for Type A samples..... 27
Figure 3.5: TGO Stress versus life fraction for Type B samples..... 27
Figure 3.6: Cross-sectional SEM of Type A TBC sample in the as-received condition 28
Figure 3.7: Cross-sectional SEM of sample A1 post furnace cycling 28
Figure 3.8: Cross-sectional SEM of sample A3 post furnace cycling 29
Figure 3.9: Cross-sectional SEM of Type B TBC sample in the as-received condition 29
Figure 3.10: Cross-sectional SEM of sample B2 post furnace cycling 30
Figure 3.11: Cross-sectional SEM of sample B5 post furnace cycling 30
Figure 4.1: Baseline curve at condition B compared to the multiple amplitude tests 42
Figure 4.2: SEM cross-section of as-received Type A sample.. 43
Figure 4.3: SEM cross-section of sample A1 44
Figure 4.4: SEM cross-section of sample A3 45
Figure 4.5: X-Ray diffraction on spalled Type A sample..... 46
Figure 4.6: SEM cross-section of as-received Type B sample 47
Figure 4.7: SEM cross-section of sample B2..... 48
Figure 4.8: SEM cross-section of sample B5 49
Figure 4.9: X-Ray diffraction on spalled Type B sample. 50

Table I: Composition and thickness of Type I and Type II TBC's [25] 14
Table II: Composition and thickness of Type A and Type B samples 14
Table III: Spallation Lives of Type I TBC's Subjected to Multiple Temperature Tests [25] 31
Table IV: Spallation Lives of Type I TBC's Subjected to Multiple Hold Time Tests [25] 31
Table V: Spallation Lives of Type II TBC's Subjected to Multiple Temperature Tests [25] 32
Table VI: Linear Damage Coefficients for Type I TBC's [25] 51
Table VII: Linear Damage Coefficients for Type II TBC's [25] 52
Table VIII: Total life fractions for multiple amplitude tests for Type I TBC's and error on total and predicted life 52
Table IX: Stress offset, total life fractions, and error for multiple amplitude tests 53

Abstract

Thermal barrier coatings (TBCs) are important in increasing performance and extending the life of gas turbine engine hot parts. Over the course of thermal cycling and engine operation, the coatings eventually spall off exposing superalloys to extreme temperatures. In this thesis, two aspects involving thermal barrier coating life prediction were explored. The first was by making use of stress measurements in the thermally grown oxide (TGO) to predict lives of samples subjected to non-constant furnace testing. This work used data from an earlier thesis and for the first time developed specific strategies to predict remaining life in the face of changing peak temperatures and hold times. Secondly, the relation between stress and coating life in two new coating systems was explored experimentally with furnace cycling and TGO stress measurements which was done as input for a potential industrial application to aircraft maintenance. Because there was an issue with one of the two samples types supplied, the project was expanded to understand the nature of the defect in some of the samples provided. All research was conducted in service of the goal of allowing TGO stress measurements to be used to predict remaining life of actual engine parts.

1. Introduction

In this thesis we have concentrated on various aspects of the use of PLPS for life prediction in thermal barrier coatings. In the first section, we discuss the use of data developed in a previous thesis to predict the remaining coating life under variable conditions. These results are given in sections 3.1 – 3.6. In the second part of the thesis we describe an attempt to establish the relation between measured TGO stress and spallation life for two coatings not previously characterized. These samples turned out to have highly inconsistent and low durability in cyclic furnace tests. Instead of finding this relationship, the primary results were to determine the cause of the inconsistent behavior. These results are given in section 3.7 – 3.12. The experimental methods are common to both and given in section two.

1.1 Thermal Barrier Coatings Review

Thermal barrier coatings have been developed and researched over the last half century and applied to various industries for power generation, aircraft propulsion and even naval and marine applications. With a demand to increase efficiency and power, engines were operated at higher temperatures for longer periods of time thus yielding the need for these coatings to shield the metals and alloys in turbine engines from the increasingly high temperature gas path. TBCs are multilayered complex coating systems that protect the metal from the gas path and allow materials to be used at temperatures above their melting points [Clarke *et al*; 2005, Nicholls *et al*; 2002, Jones; 1996, Padture *et al*; 2002].

Most production thermal barrier coatings consist of a four layer coating system (Figure 1.1). The first layer consists of a low thermal conductivity ceramic topcoat, typically 100-125 microns thick sitting above an oxidation and corrosion resistant bond coat. The second layer is the bond coat which is an aluminum rich layer between the topcoat and the superalloy that reacts

with oxygen during thermal cycling and forms an oxide layer above it. The bond coat ensures that the TBC is firmly mounted and provides the aluminum supply for the thermally grown oxide (TGO) to grow during exposure to high temperatures. Lastly is the metallic substrate, typically a single crystal superalloy on which the bond coat, TGO and ceramic top coat all adhere to. TBC materials must provide (1) high melting point and phase stability, (2) low thermal conductivity, (3) chemical inertness, (4) thermal expansion match between topcoat and metallic substrate, and (5) a good adherence to the metallic substrate in order to properly operate efficiently in high temperature situations [Cao *et al*; 2004].

1.1.1 Ceramic Top Coat

Various ceramics have been tried and tested in TBC systems with very few actually succeeding in properly insulating the metallic substrate from the high temperature gas path for extended periods of time. Zirconia has become the optimal choice over the last few decades due to its extremely low thermal conductivity and its high thermal expansion coefficient. In most systems, zirconia is stabilized with 6-8 wt. % Y_2O_3 (YSZ) which hinders the transformation from tetragonal to monoclinic zirconia thus reducing residual stresses and volumetric changes during high temperature cycling [Schulz *et al*; 1996]. In addition, the 6-8 wt. % ytrrium with zirconia has proven itself in thermal cycling tests with maximum life being obtained with this specific ceramic composition [Stecura; 1985]. The only other production TBC ceramic has been gadolinium zirconate which has good high temperature properties but is more expensive and has low fracture toughness.

The ceramic top coat is applied through various methods, including air plasma spray (APS) and electron beam physical vapor deposition (EB-PVD). In advanced TBC's, EB-PVD is the deposition method of choice, and all samples in this work contain ceramic top coats applied

in this manner. The process allows for a columnar grain structure of zirconia to be grown where the columns lower tensile stress build-up and alleviate the coefficient of thermal expansion differences between the TBC and the metallic substrate [Morrel, Rickerby; 1998]. In addition, only EB-PVD coatings are sufficiently transparent to allow optical access to the TGO as needed for much of the work in this thesis.

1.1.2 Bond Coat and Thermally Grown Oxide

An oxidation resistant bond coat is applied to all TBC systems to allow proper adherence of the ceramic top coat to the superalloy. Most bond coat systems have a thickness of 50-150 microns and contain an aluminum rich layer which allows for the growth of the TGO. During engine operation a highly stable aluminum oxide, α-Al_2O_3 is grown as the bond coat becomes oxidized. This layer of aluminum oxide provides protection to the bond coat and ensures a stronger bond between the alumina and zirconia ceramic top coat [Terry; 1998]. In selecting bond coats, it is highly desirable to choose a bond coat composition that will allow for the formation of the stable alpha-alumina oxide as other oxide formation in between the bond coat and top coat can lead to volumetric expansion or contraction and premature tensile cracking in the TGO separating the ceramic top coat from the rest of the system [Lipkin *et al*; 1997b]. In addition, α-Al_2O_3 is very slow growing due to the low diffusion rate of oxygen through the TGO.

Bond coat compositions vary greatly across different applications, but the most common bond coats used in industry consist of aluminide (NiAl) or MCrAlY coatings. Aluminide coatings sometimes include other materials such as platinum too allow for enhanced aluminum diffusion and stronger adherence of the oxide to the bond coat [Chen; 1997]. MCrAlY bond coats contain more elements with the M being iron, cobalt, nickel or a mixture of nickel cobalt and can be deposited regardless of the metallic substrate. Both bond coats differ in processing

with aluminide coatings being deposited by chemical vapor deposition (CVD) and diffusion processes, and MCrAlY bond coats by APS or high velocity oxygen fuel (HVOF) or low pressure plasma spray (LPPS).

1.2 Photoluminescence Piezospectroscopy (PLPS)

Photoluminescence piezospectroscopy provides a non-destructive technique to measure and determine the stress in the thermally grown oxide. The technique, invented by Paton *et* al 1997 is helpful in measuring the compressive stress within the TGO throughout thermal cycling and is based on the frequency shift in the Cr^{3+} ions. Using a 514 nm continuous laser, which corresponds to one of the absorption wavelengths of chromium in alpha-alumina, a red luminescence is producing in the TGO and two distinct peak doublets form at 14,402 cm^{-1} (R_1) and 14,432 cm^{-1} (R_2). The stress of the TGO is obtained through various software programs and depends on the R_1 and R_2 peak positions, peak intensities, and peak separation [Lipkin *et al*; 1995, Christensen *et al*; 1996, Lipkin and Clarke; 1996, Clarke *et al*; 1997]. The spectra obtained due to the TGO stress can be fit to a Gaussian-Lorentzian function to obtain the peak shift and with the use of background subtraction and least square fitting, peak position and separation can be found and related to the stress in the TGO [He and Clarke; 1995].

The PLPS technique has been used frequently on platinum aluminide bond coats and in all cases measured TGO stress shows a steady decline in stress over the life time of thermal cycling. As the TBC's are subjected to thermal cycles, the measured TGO stress increases during the initial transient phase, but then decays steadily over time until failure when stress readings are 0 GPa in the presence of pure alpha-alumina [Selcuk and Atkinson; 2003, Clarke, Xie *et al*; 2003, Sridharan *et al*; 2004, Wen *et al*; 2005].

1.3 Current Life Prediction Models

Current life prediction models for thermal barrier coatings are based on physical engineering models that make use of empirical and experimental data on similar coating systems. These models take into account the cycle life of the coatings at a certain temperature, the stress decay over cycle time, and various other degradation parameters such as TGO thickness and bond coat rumpling to try and evaluate the life of TBC systems. Various models have been produced to try and better correlate data obtained from experimental thermal cycling to better predict coating life by making use of fatigue laws. At least one model uses finite element models combined with realistic constitutive models to calculate the inelastic strain in the TBC to capture the irreversibility in the deformation [Ahmadian *et al*; 2013]. Current data has stemmed from furnace cycling and testing at constant temperatures and hold times without taking into account real life aerospace applications in which commercial and military aircraft often change routes and flight durations. It is not unusual in commercial aviation that an aircraft can be used on routes of different durations both from year to year or even on a single multi-destination flight. Military aircraft engines are likely to have even more varied operational history. In this work, tests are carried out in which the temperature history is not constant throughout the test. The peak temperature or the cycle duration was changed at roughly half the remaining life of the samples.

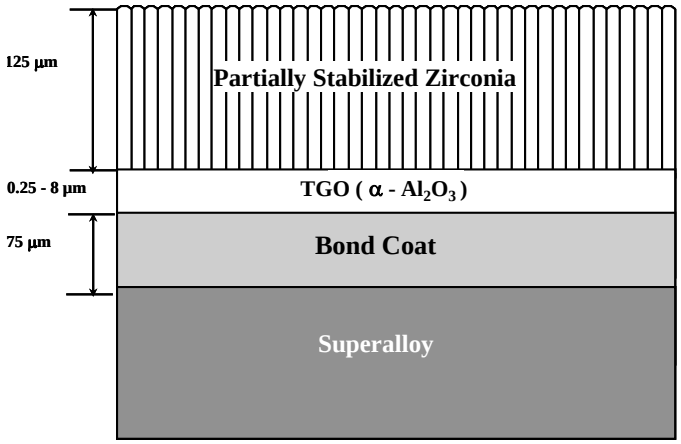

Figure 1.1: Thermal barrier coating system [25]

2. Experimental Setup

2.1 TBC Specimens

In this work, four Types of TBC specimens were examined and tested to try and measure TGO stresses during thermal cycling and to try and develop life prediction models based on the TGO stress. For the case of samples previously tested in another thesis, two Types of thermal barrier coatings were provided. Both Types consisted of coupon samples 25.4 mm in diameter and 3.2 mm in thickness coated with YSZ topcoats deposited by EB-PVD (Figure 2.1). Type I TBC samples consisted of 150 micron 7% weight Y_2O_3 (YSZ) stabilized Zirconia electron physical vapor deposited (EB-PVD) top coat, and a 75 micron grit blasted platinum nickel-aluminide bond coat [(Ni, Pt) Al]. The bond coat on Type I was outwardly grown at 1080^{o}C and grit blasted prior to electron beam physical vapor deposition (EB-PVD) of the ceramic top coat. Type II TBC consisted of 175 micron 7% weight Y_2O_3 (YSZ) stabilized Zirconia top coat, and a 55-60 micron grit blasted platinum modified nickel-aluminide bond coat. The bond coat on Type II was inwardly grown at 982^{o}C before the same EB-PVD process applied the ceramic top coat. The composition of these is shown in Table I.

For the study conducted on newer thermal barrier coating systems, two Types of TBC's were also provided. Both were coupon samples 22.5 mm in diameter and 4.5 mm in thickness. The first batch, designated as Type B contained a 140 micron thick ceramic topcoat deposited by EB-PVD. Type B samples contained a diffused platinum aluminide bond coat 62-64 microns in thickness with 20-35 wt. % aluminum and 30 wt. % platinum concentrations. The second set, designated as Type A samples contained a 135 micron thick YSZ ceramic topcoat deposited with the same EB-PVD method. In addition, Type A samples contained a 52-54 micron thick diffused

platinum aluminide bond coat with 15-25 wt. % aluminum and 15 wt. % platinum concentration. Type B and Type A sample composition is shown in Table II.

2.2 Furnace Cycling Tests

Furnace cycling tests were conducted in bottom-loading thermal cycling furnaces made by CM Furnaces Inc. The Type S thermocouple that controlled the furnace temperature was welded to the back of a superalloy dummy sample in the center of the furnace. Three additional thermocouples were mounted in three of the four corners of the furnace and agreed at steady state with the control thermocouple within 5^{o}C. The 1-hour cycles consisted of a 10-minute heat-up to the cycle temperature, followed by a dwell for 40 minutes at the temperature. The final step was a 10-minute forced-air quench (Figure 2.2). The 24-hour cycle test consisted of the same 10-minute heat up to temperature, followed by a 1430-minute hold and then a 10-minute forced air quench (Figure 2.3)

For Type I and Type II samples, furnace cycling was conducted at 1121^{o}C and 1151^{o}C using both 1-hour and 24-hour cycles. In addition, Type I and Type II samples were subjected to two-stage cycling tests where samples were first cycled at a test condition which will be referred to as condition A until approximately fifty percent life, and then tested at a second test condition to be called B until failure. The order in which the conditions are applied is likely to matter and this is consistently designated as condition A first followed by condition B. Initial baseline testing, reported in [19] involved cycling samples at 1121^{o}C and 1151^{o}C using 1 hour and 24-hour hold times to determine the average failure life of specimens. For Type I TBC's, 11 were cycled at 1121^{o}C and nine at 1151^{o}C all using 1-hour hold times. In addition, eight were cycled at 1121^{o}C using 24-hour hold time. For Type II TBC's, six were cycled at 1121^{o}C and four at 1151^{o}C using 1-hour hold times while two were cycled at 1121^{o}C using 24-hour hold times. The

average lives of samples were used to identify approximately 50% life fraction when running two stage tests switching from test condition A to B.

For furnace cycling of Type B samples, eight specimens were cycled at 1121^{o}C using 1-hour cycles. As for Type A samples, due to the small supply of specimens, two were cycled using the same procedure as Type B samples.

2.2.1 Multiple Amplitude Testing

For the multiple temperature tests, two Types of testing procedures were utilized, tests in which samples were subjected to 1121^{o}C until about half the expected life followed by 1151^{o}C and the reverse procedure. For the multiple hold time tests, two tests were used all at 1121^{o}C in which cycling was done using 1-hour hold times for the first half and then changed to 24-hours until failure, and the reverse order.

2.3 Photoluminescence Piezospectroscopy Procedure

Photoluminescence piezospectroscopy was utilized throughout the duration of furnace cycling tests on Type A, Type B, Type I and Type II samples to determine the stresses in the thermally grown oxide during thermal cycling.

For the samples conducted in a previous study, PLPS measurements were also made throughout the duration of furnace cycling. The stress measurements were made using a Renishaw^{TM} Ramascope^{TM} 2000 system using a 514 nm laser to stimulate fluorescence. To obtain this peak shift the R1 and R2 spectra are fit to a Gaussian-Lorentzian function using Grams 32 ^{TM} Spectral Notebase software that automatically does a parabolic background subtraction. To fit the spectra, the relation between the position of the R1 and R2 peak is enforced and then least square fitting is applied. The spectra were collected on 40 random locations on each thermal barrier coating sample and the average stress values and standard

deviations were extracted to produce stress measurements as a function of thermal cycles and life fraction.

Measurements on Type A and Type B samples were made using a 250 mW continuous diode laser providing excitation of the TGO at 532 nm (Figure 2.4). The fluorescence of the chromium around 694 nm was collected and channeled to an Ocean Optics USB4000 spectrometer calibrated to measure spectra from 665-720 nm [Hawron; 2014]. Throughout cycling, measurements were made at specific intervals to properly obtain stress versus life fraction data for both Type A and Type B samples. PLPS was conducted at 0, 1, 2, 5, 10, 20, 40, 60, 100, 140, 180 etc. cycles until failure of the samples. In all cases, measurements were made using a raster scan in a 10 cm^2 area on each coupon sample. The signal was analyzed and deconvoluted into two peaks, R_1 and R_2 from which the stress was obtained due to the frequency shift and intensities of the peaks being compared to a zero stress alumina sample.

2.4 Sample Preparation for Microscopy

Standard metallographic techniques were utilized in the preparation and handling of all samples for microscopy. Specimen sectioning, mounting in epoxy, and grinding was performed on samples to obtain various images using a scanning electron microscope (SEM).

2.4.1 Sectioning, Mounting and Grinding

For Type A and Type B samples, various samples were sectioned using a high speed diamond saw to examine the microstructure and layers within the thermal barrier coating. Samples were taken as-received and post failure from thermal cycling and cut into smaller sections to obtain cross sectional pieces that can be viewed using a SEM. Once cut, the samples were mounted into Buehler's EpoThin^R epoxy resin and allowed to dry and cure for eight hours before being removed. This process ensures that the thermally grown oxide and bond coat

remain intact and that any cracking or impurities in these layers be viewed. Once mounted, samples were ground using 60, 120, 300, 600, and 1200 grit silicon carbide polishing papers with water being applied throughout the process. In addition, fine polishing was performed using 6 µm and 1 µm diamond polishing disk with diamond paste being applied on the disk. Previous polishing methods utilized were not acceptable for these samples. Due to the nature of the bond coats, cutting had to be performed using slower speeds and feeds and polishing was done as stated previously but conducted for twice the amount of time as compared to other TBC samples. Figure 2.5 highlights the cracking in the bond coat that arises from not properly polishing Type A and B samples.

2.4.2 Scanning Electron Microscopy

Once mounted and polished properly, the Type A and Type B samples were coated with a conductive gold palladium layer and observed in Jeol and Philips scanning electron microscopes. The SEM was used to observe failure modes and composition of the Type A and Type B bond coats. In addition, energy-dispersive X-ray spectroscopy (EDX) was used to identify the elemental composition of each sample. Element mapping was performed on the bond coats to identify specific concentrations of elements and point scans were also conducted in various locations to measure elements and identify possible failure mechanisms in the TBC layers. Type A and Type B coating lives were highly inconsistent and thus examined to try and determine the cause of the behavior.

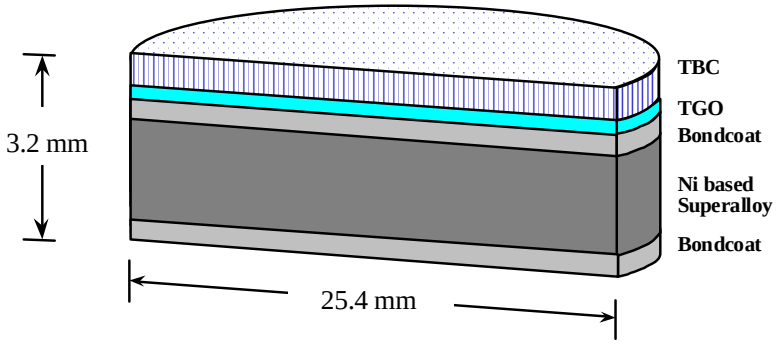

Figure 2.1: Type I and Type II TBC coupon sample geometry [25]

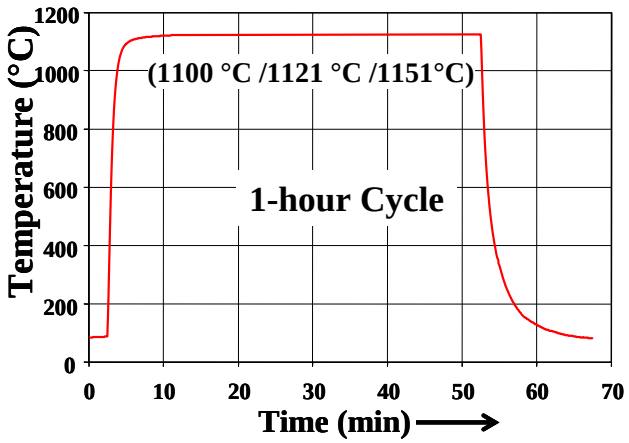

Figure 2.2: Furnace cycle temperature profile for 1-hour cyclic tests [25]

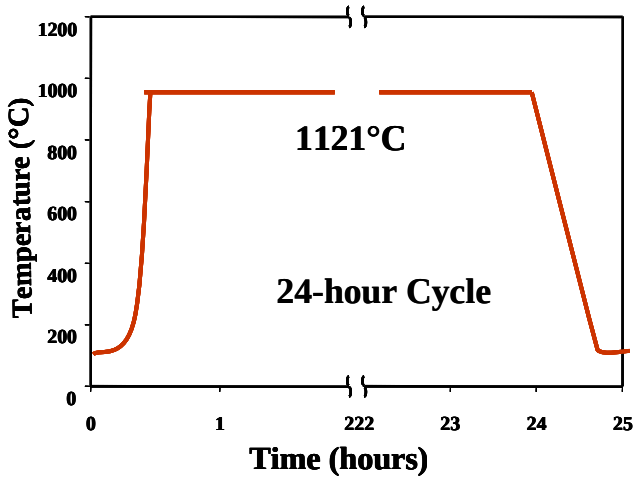

Figure 2.3: Furnace cycle temperature profile for 24-hour cyclic tests [25]

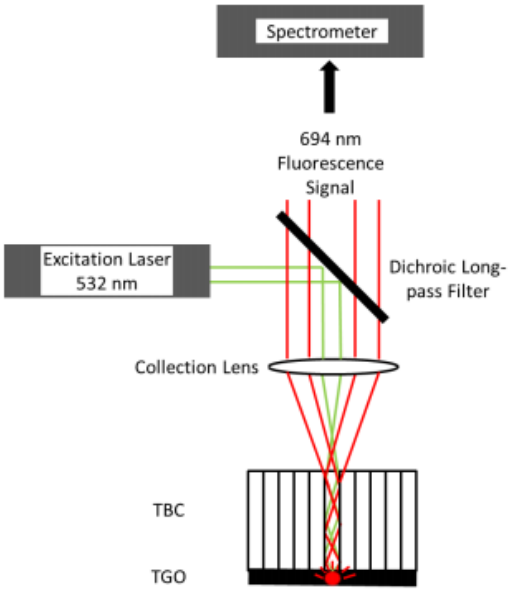

Figure 2.4: Schematic for the PLPS setup used on Type B and Type A samples [23]

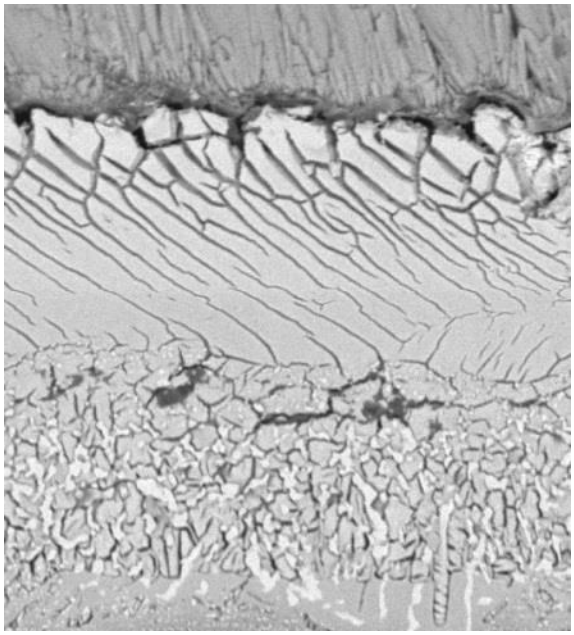

Figure 2.5: Cracking in the bond coat during polishing of Type A and B TBCs

Table I: Composition and thickness of Type I and Type II TBC's [25]

Type	Superalloy Substrate	Bond Coat		Ceramic (7 YSZ)	
		Type	Thickness (μm)	Type	Thickness (μm)
I	Single Crystal CMSX-4	Grit Blasted on Ouward Diffusing Single Phase Platinum Modified Nickel Aluminide	75	EB-PVD	150
II	Single Crystal CMSX-4	Grit Blasted on Inward Diffusing Type Single Phase Platinum Modified Nickel Aluminide	55-60	EB-PVD	175

Table II: Composition and thickness of Type A and Type B samples

Type	Bond Coat Composition (thickness μm)	Top Coat Composition (thickness μm)
Type A	53	135
Type B	62-64	138

3. Experimental Results

The experimental results from the previous study conducted on Type I and Type II TBC's are presented first, followed by the experimental results on the new Type A and Type B TBC specimens. Spallation criterion for the TBC samples was defined as a separation of the ceramic YSZ top coat from the bond coat with more than 50% removed from the substrate. Samples were monitored periodically to best obtain the number of cycles at failure.

3.1 Type I TBC Spallation Lives in Constant Cycles

For the baseline testing to determine the expected life at a certain temperature or hold time, data previously generated and presented in [19] was used. The average spallation life was 677 cycles for the eleven samples held at 1121^{o}C for 1-hour hold times and 358 cycles for the nine samples held at 1151^{o}C for 1-hour hold times. For the eight samples run at 24 hour hold times at 1121^{o}C, the average life was found to be 45 cycles.

3.2 Type I TBC Spallation Lives in Multiple Amplitude Tests

Six Type I samples underwent multiple amplitude furnace cycling in which the temperature and cycle duration were changed part-way through the cycling. Table III highlights the four samples subjected to multiple temperatures and the associated cycles for each test. Table IV shows the cycle history for the two samples subjected to a change in cycle duration and the respective cycles at each specific condition. Using constant cycle data at each temperature and hold time, tests were switched from condition A to B at approximately 50% life fraction of condition A.

3.3 Type I TBC TGO Stress as a Function of Life Fraction for Multiple History Tests

All experimental work in section 3.3-3.6 are taken from the thesis of Sridharan [25]. PLPS measurements were conducted on the thermally cycled TBC specimens at periodic intervals. The average TGO stress versus life fraction for the four samples that were subjected to multiple-temperature tests is shown in Figure 3.1 along with the 1121^{o}C and 1151^{o}C 1-hour hold time baseline tests. For the multi-temperature tests in which the samples were cycled each to half their cyclic life at 1121^{o}C using 1-hour cycles and then cycled to failure at 1151^{o}C, the slope of the TGO stress curve remaining unchanged during the transition to the new temperature, and then decreased monotonically over time. For the tests carried out at 1151^{o}C followed by 1121^{o}C, the stress versus life fraction curve remained constant during the transition to the new temperature and remained mostly unchanged.

Figure 3.2 is a plot of the TGO stress versus life fraction for the two samples that were subjected to the multiple hold time tests with a single maximum temperature of 1121^{o}C alongside the baseline 1-hour and 24-hour 1121^{o}C tests. It is clear from the figure that these tests are not single valued independent of the hold time. This is not surprising because for tests run to failure at a single hold time the curves are not independent of hold time. The possible interpretations of the behavior in Figure 3.2 will be presented in the discussion section.

3.4 Type II TBC Spallation Lives in Constant Cycles

Similar to Type I TBC's, baseline testing was conducted previously [2] on various Type II TBC samples to determine the average life at various temperatures and hold times. The average life of the six samples cycled using 1 hour 1121^{o}C tests, was 563 cycles, while for the four samples using 1151^{o}C tests, average life was 363 cycles.

3.5 Type II TBC Spallation Lives in Multiple Temperature Tests

Both Type II TBC's subjected to multiple amplitude tests underwent changes in cycle temperature. The test conditions and cycles for each test are summarized in Table V. Samples were cycled to approximately 50% life fraction at condition A, and then to failure at condition B using average spallation data obtained from constant cycling.

3.6 Type II TBC TGO Stress as a Function of Life Fraction for Multiple History Tests

The result for Type II TBC TGO stress versus life fraction is plotted in Figure 3.3 alongside baseline 1121^{o}C and 1151^{o}C 1-hour tests. For the tests carried out at 1121^{o}C followed by 1151^{o}C, there was an increase in the stress of the sample during the transition to the higher test temperature, but the stress eventually decreased and remained relatively unchanged to failure. A different trend was noted for the tests carried out at 1151^{o}C followed by 1121^{o}C. The rate of change of TGO stress was left mostly unchanged during the transition to 1121^{o}C and was not as substantial as that for tests carried out at 1121^{o}C followed by 1151^{o}C.

3.7 Type A TBC Spallation Lives

All furnace cycling conducted on Type A samples was done using 1-hour cycles at 1121^{o}C. Two samples were cycled in the furnace and monitored periodically for spallation of the ceramic top coat from the bond coat. The average furnace cycle life was 190 1-hour cycles with Type A sample A1 failing at 220 cycles and Type A sample A3 failing at 160 cycles. Compared to the previous study conducted on similar thermal barrier coating specimens, failure life was found to be relatively inconsistent and premature with the Type A samples.

3.8 Type A TGO Stress as a Function of Life Fraction

PLPS stress measurements were conducted regularly on Type A samples throughout the duration of furnace cycling. The results for Type A TGO stress versus life fraction are plotted in Figure 3.4. The samples experienced a slight rise in stress during the transient cycling phase, and then gradually decreased to around 1.0 GPa near failure. Both samples followed a similar trend with the initial stress ranging from 1.5-2.0 GPa and then following a monotonic decay to failure.

3.9 Type B TBC Spallation Lives

Similarly to Type A TBC samples, all Type B samples were cycled in the same furnace using the same 1-hour cycles at 1121^{o}C. For Type B samples, cyclic life was scattered and the average failure lives of samples was found to be 218 1-hour cycles. Samples B2 and B6 lasted the longest at 520 and 320 cycles respectively, while samples B1, B4, B7 and B8 lasted at 190, 120, 80, and 80 cycles respectively. Once again, this newer coating system was shown to be inconsistent with respect to PLPS behavior and consists of most samples failing prematurely and a large deviation of failure lives.

3.10 Type B TGO Stress as a Function of Life Fraction

Figure 3.5 highlights the TGO stress as a function of life fraction for all Type B cycled at 1121^{o}C using 1-hour cycles. Unlike Type A samples, the stress values were much higher with average initial stress in the range of 2.5 GPa. In addition, the samples experienced much less decay in stress throughout cycling with failure occurring at relatively high stresses of 1.7-2.4 GPa. Type B TGO stress did not follow much of a monotonic decay in stress with samples experiencing stress relaxation less than 30% during the course of furnace cycling.

3.11 Scanning Electron Microscopy of Type A Samples

3.11.1 SEM of As-Received Type A Sample

The various layers of the newer thermal barrier coating systems were observed in a scanning electron microscope to observe and quantify the bond coat layers and composition along with the TGO thickness and top coat dimensions. A cross-sectional picture of an uncycled as-received Type A sample is shown in Figure 3.6. As shown, the bond coat contains a two layer composition with element segregation in the bottom layer. The top layer is mostly uniform while heavier elements, circled in red, are non-homogenous and scattered in the lower bond coat layer. In addition, a very thin TGO layer, about 0.5 μm in thickness, is found throughout the uncycled sample. The TGO is generally uniform in thickness, but due to the large undulations in the bond coat, certain areas reached 5 μm in thickness.

3.11.2 SEM of Type A Sample A1 (220 cyclic life)

The microstructure of the thermally cycled Type A samples was observed using a scanning electron microscope as well to examine and study the TGO growth, ceramic top coat/TGO interface, and the TGO/bond coat interface. Figure 3.7 shows sample A1, which after being subjected to 1-hour cycles at 1121^{o}C, failed prematurely at 220 cycles.

Once again, the heavy element segregation is shown to appear in the bottom layer of the bond coat as the lighter spots indicate atomically heavier elements. In this region, they are separated and distributed throughout the layer and oxidize during the course of cycling. Furthermore, with continued furnace cycling, the TGO has grown and increased in thickness. Shown as the dark material sitting above the bond coat, the thickness of the TGO varies throughout the Type A sample with some regions displaying thickness as big as 10 μm and some

areas as small as 4 µm. Critical TGO thickness at failure is not observed for this TBC due to the large variations in thickness.

The interface between the bond coat and the TGO was also found to change with furnace cycling. The undulations seen in an uncycled sample had grown, and the TGO was found to grow inwardly into the bond coat. The undulations shown in Figure 3.6 increased as TGO growth continued and left large ridges as shown with in Figure 3.7. This inward displacement of the TGO into the bond coat is often referred to as rumpling [Pennefather and Boone; 1994] and in Type A 1 reached maximum peak to valley measurements of 12 µm. This measurement was found as the maximum when scanning across the length of the cross-section.

3.11.3 SEM of Type A Sample A3 (160 cyclic life)

Sample Type A3 was also examined following failure from furnace cycling in the scanning electron microscope to observe and examine the TBC interface layers and TGO thickness. Shown in Figure 3.8 premature failure was shown once again in this sample as it failed at 160 cycles during 1-hour cycling at 1121^{o}C. Similarly to A1, and the as-received A4, heavy element segregation was contained in the lower layer of the bond coat, as seen in the uncycled sample, and lasted throughout the duration of furnace cycling. Furthermore, the TGO layer continued to grow during cycling and varied greatly in thickness throughout the sample above the bond coat. In some regions, TGO thickness was seen to be quite small around 2-4 µm, but in other areas was upwards of 10 µm in thickness.

During the course of furnace cycling, the bond coat continued to cave inwards in certain areas and gave way to thicker areas of TGO growth above these inward displacements. These areas are scattered throughout the sample and are highlighted by valleys in the bond coat where

TGO growth reached 10 µm and greater. The increased undulations within the bond coat, and the varying TGO thickness may be a factor in the premature failure of Type A samples.

3.12 Scanning Electron Microscopy of Type B Samples

3.12.1 SEM of As-Received Type B Sample

A cross-section scanning electron microscope image of an uncycled as-received Type B sample is shown in Figure 3.9. The bond coat here contains two distinct layers each with a different atomic concentration. Below the ceramic YSZ top coat is a much lighter region. This top layer bond coat is rich in heavier elements compared to the lower bond coat layer. In addition, unlike Type A samples that saw heavy element segregation, the Type B samples exhibit homogenous distribution of heavy elements in the top bond coat layer. Underneath the initial bond coat layer is a second layer consisting of atomically lighter elements homogenously distributed throughout the sample. The TGO thickness in the as-received Type B sample was generally less than 0.5 µm throughout the sample and didn't experience a large variation in thickness like that of Type A samples. Bond coat displacements were much less and maximum inward displacements of the TGO in the bond coat were found to be around 1 µm compared to 5 µm for Type A samples.

3.12.2 SEM of Type B Sample B2 (520 cyclic life)

The microstructure of Type B samples was found to be quite different from that of Type A samples in the as-received condition and following thermal cycling at 1121^{o}C. Figure 3.10 highlights the evolution of the TGO with thermal cycling on B2 which had the longest cyclic life at 520 cycles.

The first noticeable aspect of sample B2 is the heavy element segregation that developed during cycling. These white shapes spread throughout the bond coat layers formed and began moving upwards towards the bond coat/YSZ surface. The heavy elements are non-homogenous, and occur sporadically throughout the top bond coat layer, but are much more consistent in the lower bond coat layer. Type B samples before thermal cycling did not display element segregation, but contained a more consistent two layered bond coat with heavier elements in the top layer.

In addition, the TGO grown during furnace cycling was non-uniform in thickness. In certain areas, TGO thickness was greater than 10 µm and displayed brittle behavior with cracking and rolling above the bond coat. On the other hand, certain areas contained a TGO less than 4 µm thick and thus critical TGO thickness at failure was not observed. Rumpling was also observed in sample B2 and is highlighted in Figure 3.10. Bond coat displacements varied throughout the sample but in some regions was 10 µm from peak to valley and contained a thick TGO above it.

3.12.3 SEM of Type B Sample B5 (80 cyclic life)

The microstructure and evolution of TGO with thermal cycling for sample B5 is shown in Figure 3.11. Type B 5 failed at 80 1-hour cycles at 1121^{o}C. The failure lives in Type B and Type A samples have been inconsistent in the number of cycles and vary greatly between different sample types. Some similarities were observed between sample B5 and B2 in the TGO and overall bond coat response to thermal cycling.

Firstly, heavy elements began to arise and were scattered among the top layer of the bond coat in sample B5. The separation was non-homogenous and spread unevenly throughout the bond coat with larger concentrations of heavy elements in the lower bond coat layer.

Furthermore, the TGO was non-uniform in thickness and displayed brittle behavior with cracking and sand-like granules. TGO thickness was also generally non-uniform and in some areas was as low as 4 μm or as thick as 12 μm in other areas.

The final observation was the inwards displacements of the bond coat in which thick TGO growth was observed. The rumpling of the bond coat varied across the sample, but in all cases contained thick layers of TGO above it. The rumpling of the bond coat was observed at maximum to be around 5-8 μm from peak to valley.

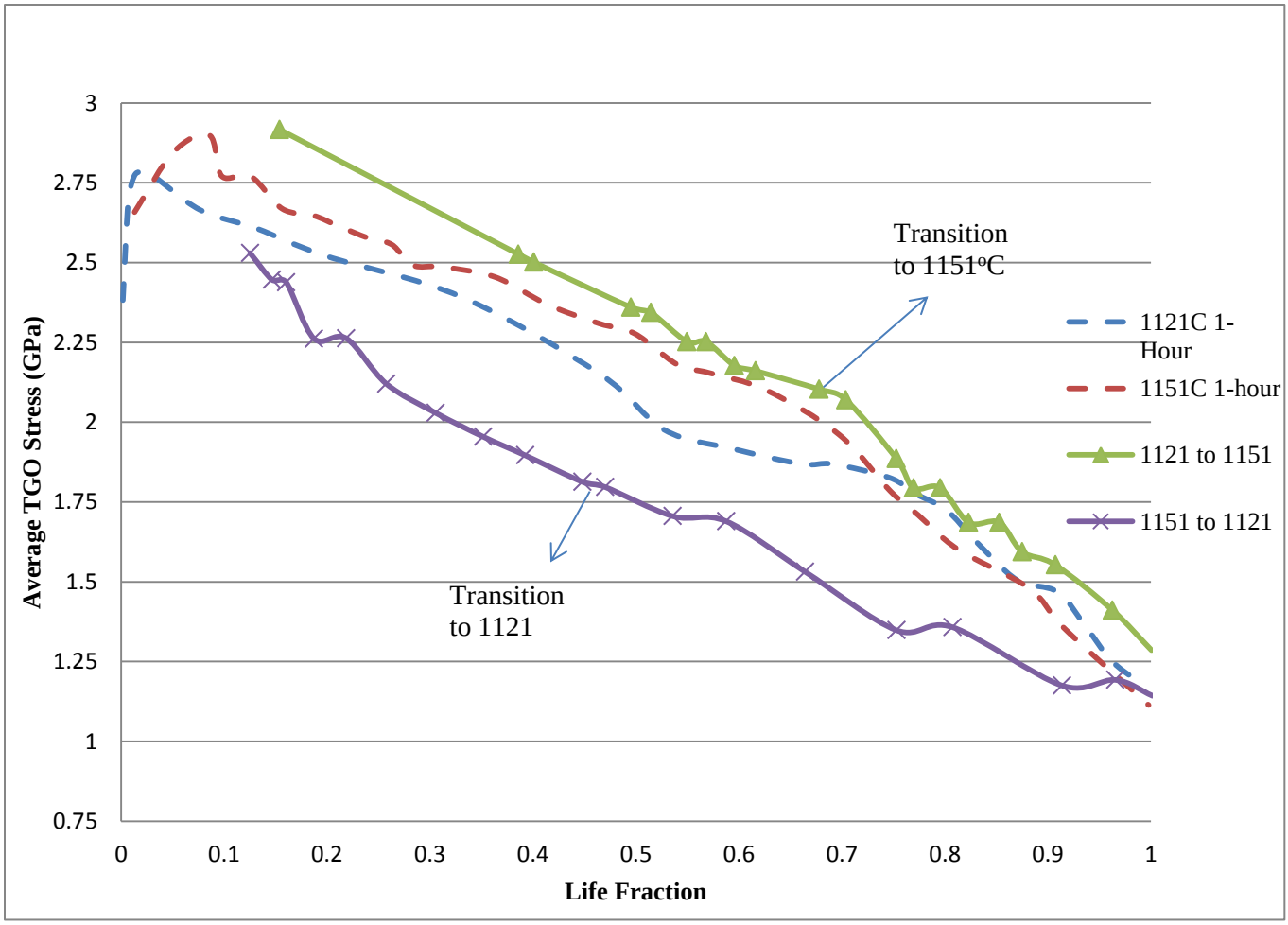

Figure 3.1: TGO stress as a function of life fraction at 1121°C and 1151°C for Type I TBC samples

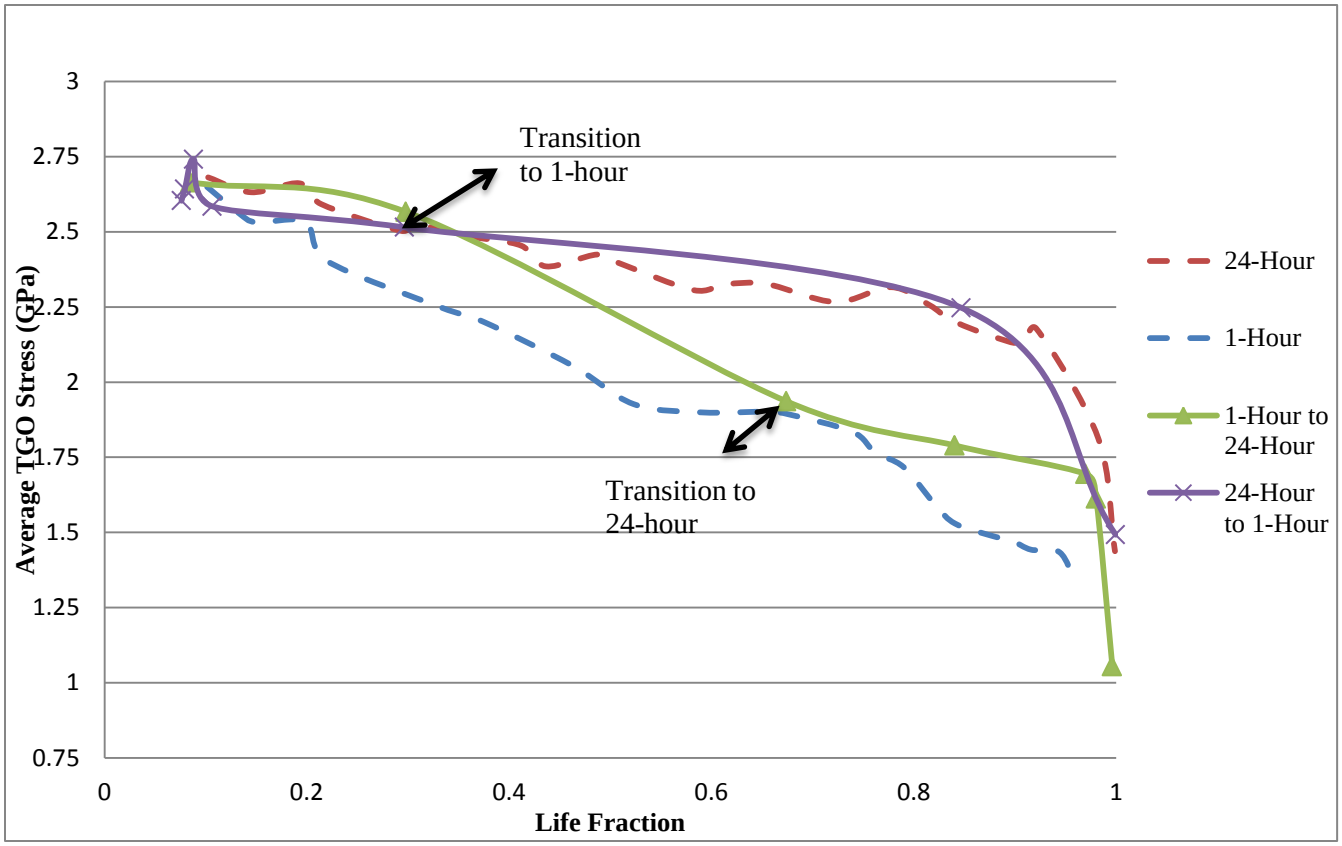

Figure 3.2: TGO Stress as a function of life fraction at 1121^{o}C for Type I TBC samples

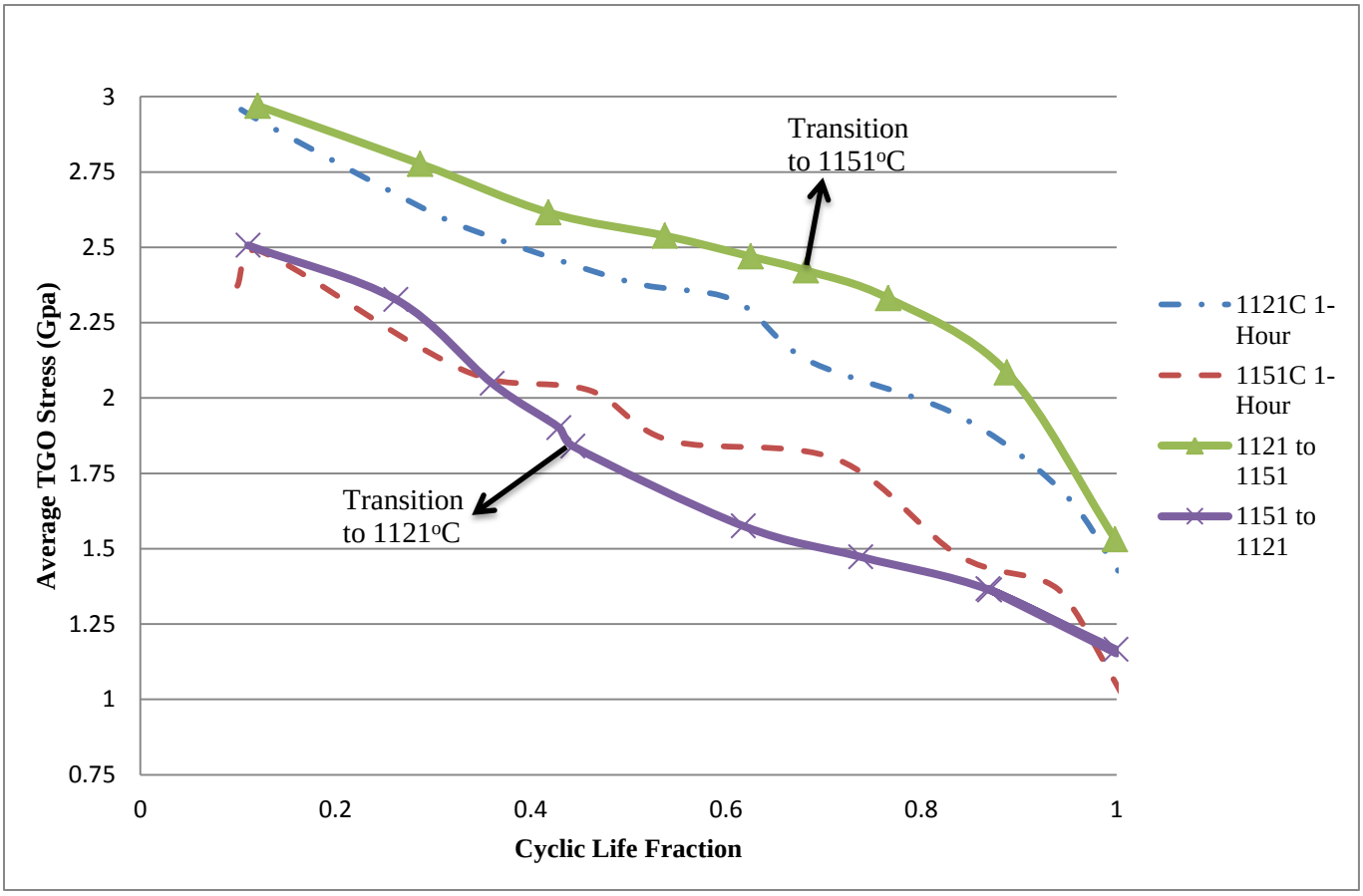

Figure 3.3: TGO Stress as a function of life fraction at 1121°C and 1151°C for Type II TBC samples

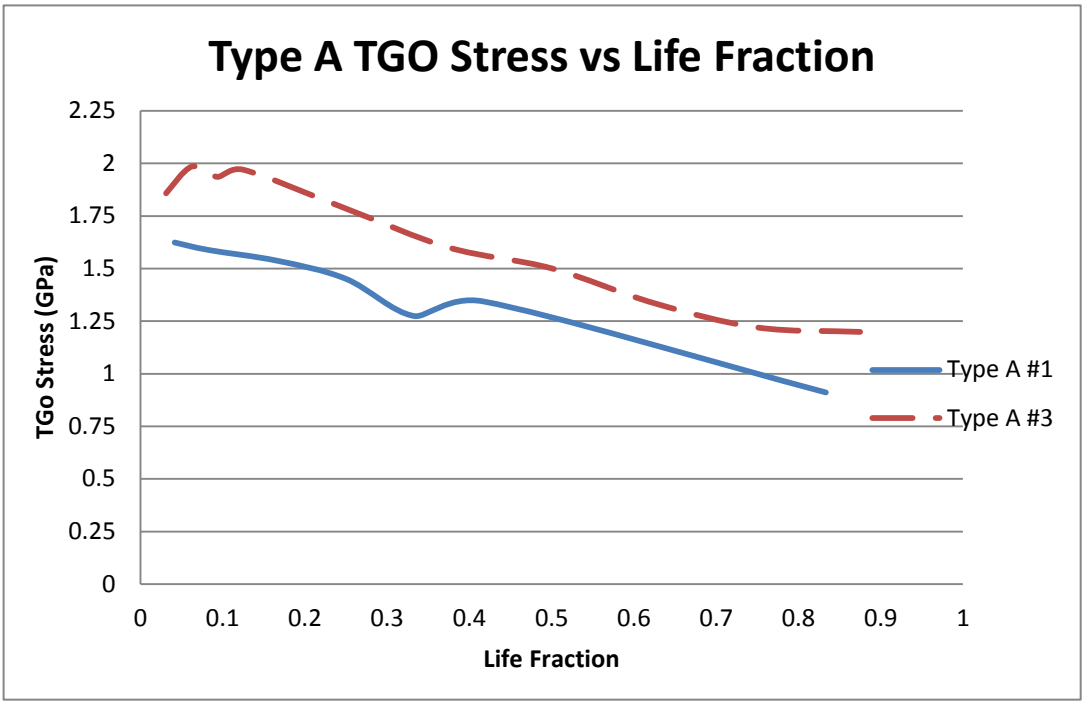

Figure 3.4: TGO Stress versus life fraction for Type A samples

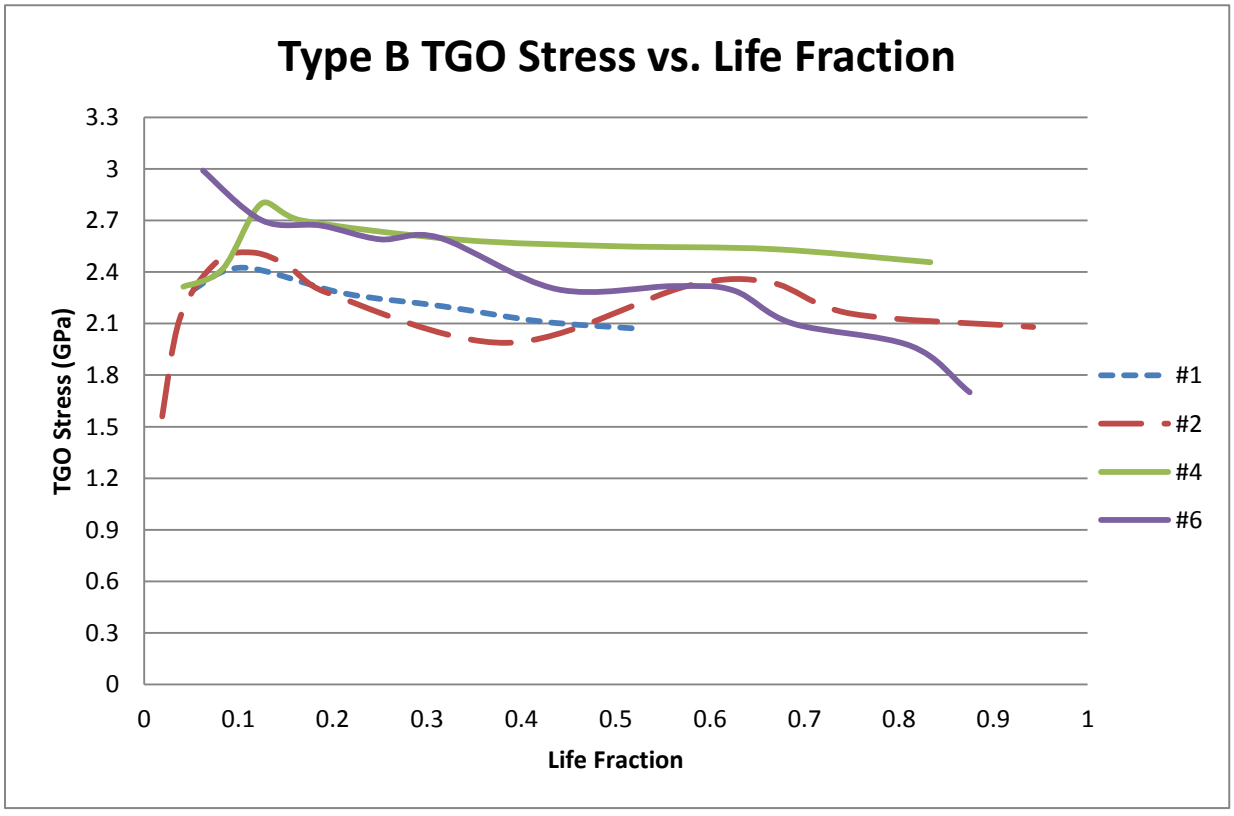

Figure 3.5: TGO Stress versus life fraction for Type B samples

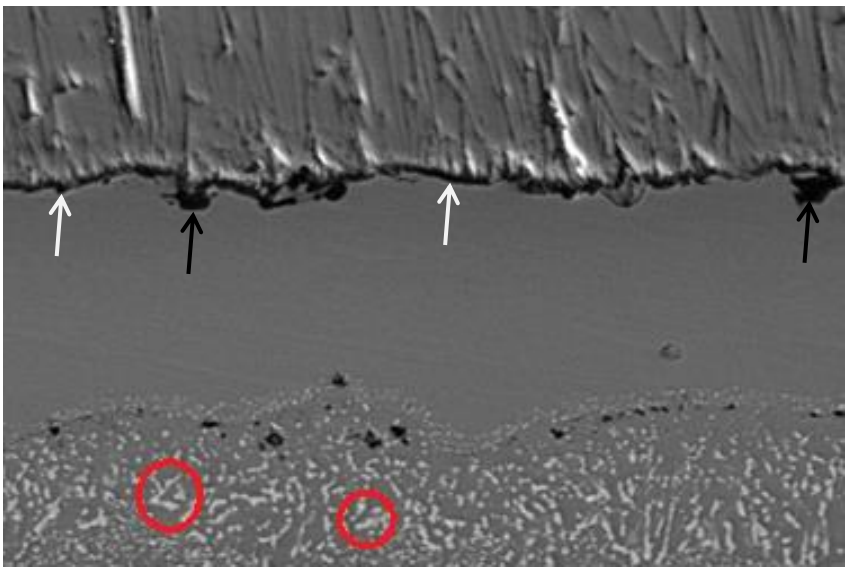

Figure 3.6: Cross-sectional SEM of Type A TBC sample in the as-received condition. Red circles highlight the heavy element segregation in the bottom bond coat layer. White arrows point to the TGO, and black arrows show the undulations between the TBC and bond coat.

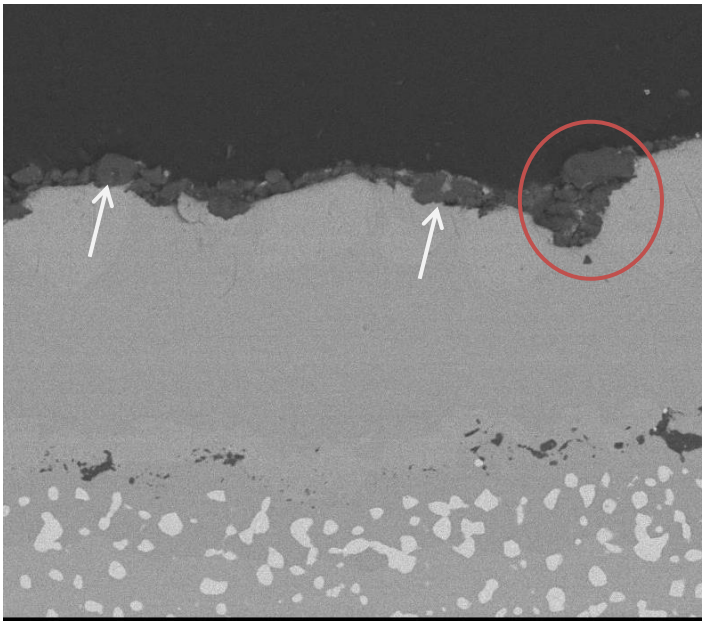

Figure 3.7: Cross-sectional SEM of Type A sample A1 post failure from furnace cycling. Heavy element segregation is still prevalent in the lower bond coat layer. The TGO layer, above the bond coat, is shown with white arrows while the inward displacement of the TGO into the bond coat is circled in red.

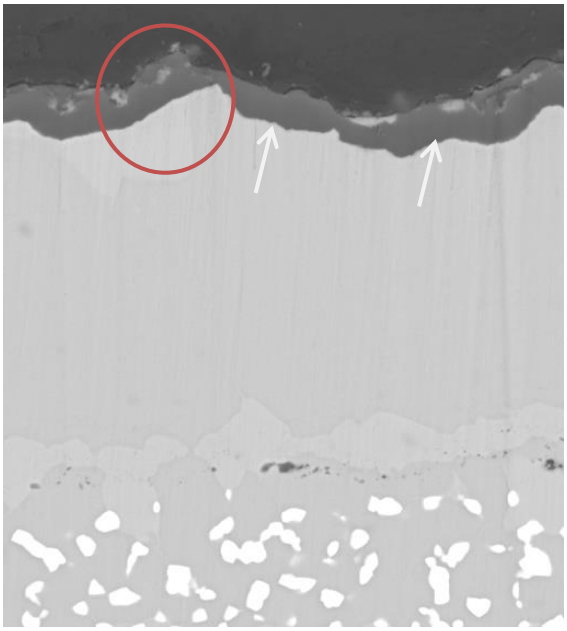

Figure 3.8: Cross-sectional SEM of Type A sample A3 following thermal cycling. The TGO layer, shown with arrows is distributed along the sample with varying thickness. The large inward displacements of the bond coat give way to thicker TGO growth as shown in red.

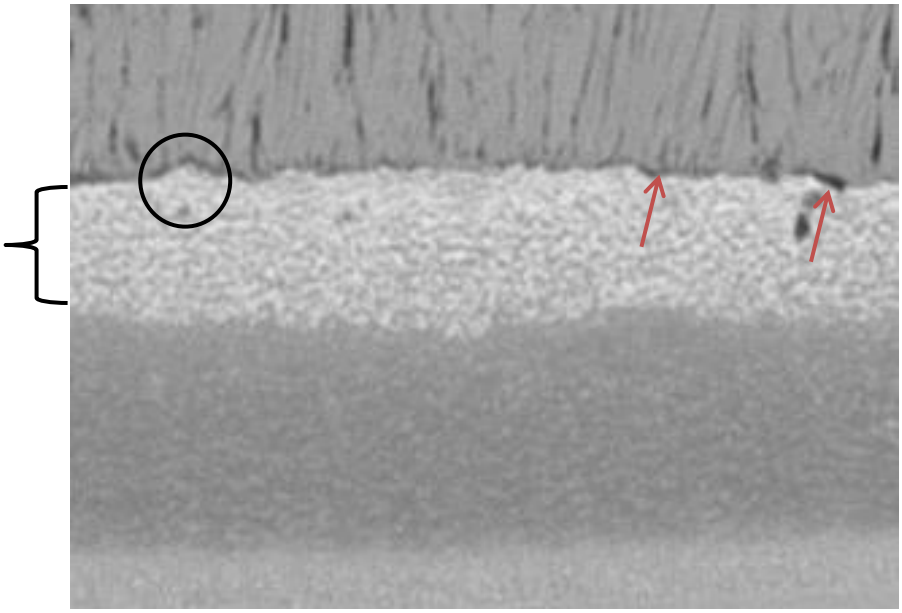

Figure 3.9: Cross-sectional SEM of Type B TBC sample in the as-received condition. The black brace highlights the top bond coat layer with heavier elements. Red arrows point to the TGO, and circled in black is an undulation between the TBC and bond coat.

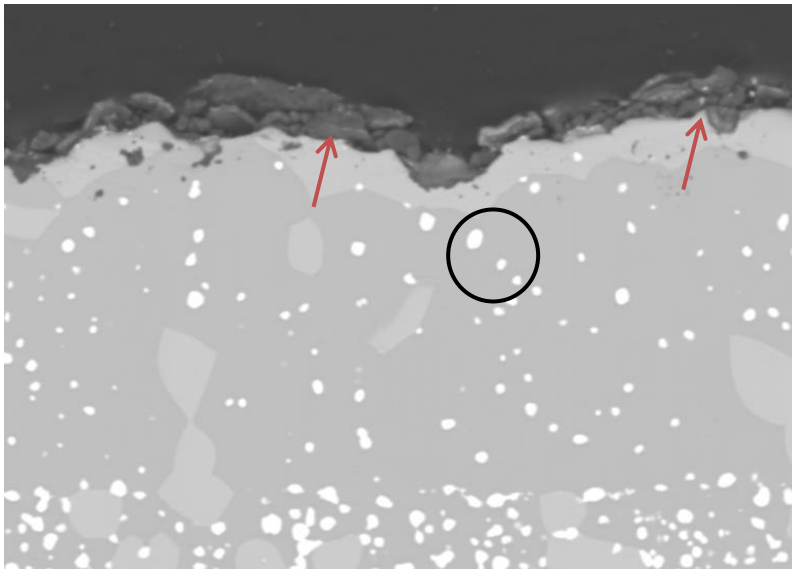

Figure 3.10: Type B sample B2 SEM cross-section following thermal cycling. Heavy element segregation is shown in black with the red arrows pointing to the TGO. TGO growth in this sample was brittle and varied in thickness.

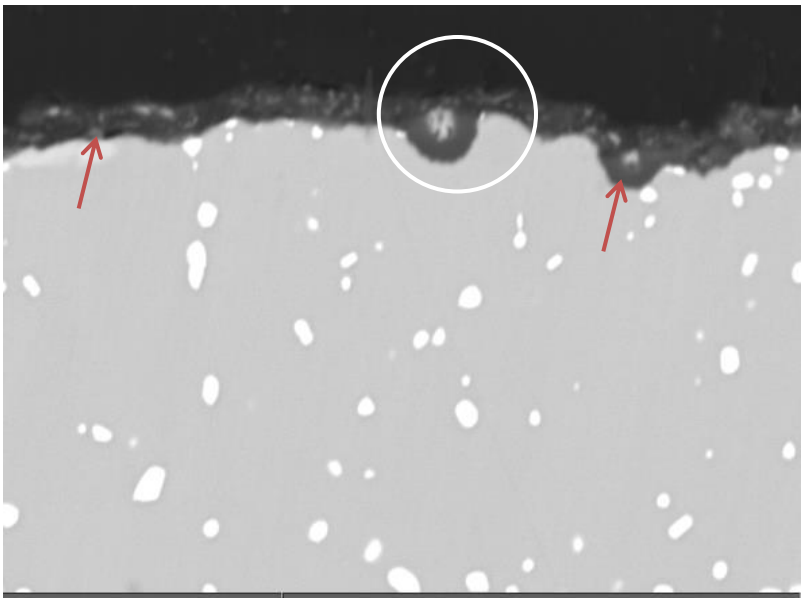

Figure 3.11: Type B sample B5 cross-section following thermal cycling. TGO is shown with red arrows and bond coat rumpling is highlighted in white. Heavy element segregation is shown once again scattered throughout the bond coat.

Table III: Spallation Lives of Type I TBC's Subjected to Multiple Temperature Tests [25]

Sample	**First Exposure Temperature, T_1 (°C)**	**Second Exposure Temperature, T_2 (°C)**
LD 73	1121°C	1151°C
# Cycles at each Temperature	335	205 (Failed)
LD 74	1121°C	1151°C
# Cycles at each Temperature	335	225(Failed)
LD 82	1151°C	1121°C
# Cycles at each Temperature	185	340(Failed)
LD 84	1151°C	1121°C
# Cycles at each Temperature	185	409(Failed)

Table IV: Spallation Lives of Type I TBC's Subjected to Multiple Hold Time Tests [25]

Sample	**First Hold Time, t_1 (minutes)**	**Second Hold Time, t_2 (minutes)**
LE 33	45	1425
# Cycles at each Hold Time	345	11 (Failed)
LE 04	1425	45
# Cycles at each Hold Time	22	298(Failed)

Table V: Spallation Lives of Type II TBC's Subjected to Multiple Temperature Tests [25]

Sample	**First Exposure Temperature, T_1 (°C)**	**Second Exposure Temperature, T_2 (°C)**
LV 37	1121°C	1151°C
# Cycles at each Temperature	261	157 (Failed)
LV 48	1151°C	1121°C
# Cycles at each Temperature	165	218 (Failed)

4. Discussion

The following results and error in life prediction for all cases are based on total life error. The measurements were made with regards to the total remaining life in each of the multiple amplitude tests and are represented in this way. For life prediction scenarios, the error on the remaining life will also be given in parentheses. When dealing with the life prediction error on the remaining life, error is roughly twice as high as the total life error due to taking into account the remaining life at the point of transitioning from test condition A to B.

4.1 Linear Damage Rule for Type I and Type II TBC's

For the first time, multi-stage furnace cycling tests were conducted [25] to try and validate the linear damage rule to better predict the remaining life of the TBC samples. The linear damage rule in this case is given as Equation 1 where D represents the predicted life fraction at failure. It is desired that damage, D, be equal to one at the end of life for the linear damage rule to be satisfied. Damage was calculated for each specimen that underwent two stage furnace cycle testing. For the tests, when D>1 the linear damage rule predicts the part to have failed prior to its actual end of life and hence is conservative. Correspondingly, for D<1 at the end of life, the linear damage rule over predicted the remaining life and is non conservative. In the following analysis, we use all the average life values in the linear damage rule. The actual damage, D at failure is given in Table VI and VII for Type I and II TBC's where the damage fractions at each specific stage are calculated from the fractions in Equation 1.

$$D = \frac{Cycles\ at\ Condion\ A}{Average\ Cycles\ to\ Failure\ at\ A} + \frac{Cycles\ at\ Condition\ B}{Average\ Cycles\ to\ Failure\ at\ B}$$

Equation 1: Linear Damage Rule Equation for Multi-amplitude Tests

First, for the Type I specimens undergoing multi-temperature tests, the linear damage rule is reasonably satisfied. Samples subjected to this loading condition ranged from 1.018 to 1.122 for total TBC damage yielding a conservative life prediction. For the Type I samples subjected to multiple hold times, the linear damage rule is satisfied when LE 04 underwent 24-hour cycles followed by 1-hour cycles at 1121^{o}C. The total TBC damage fraction was found to be 0.928. However, for sample LE 33 that underwent 1-hour cycles followed by 24-hour cycles, TBC life fraction was found to be 0.753 suggesting that one hour cycles are more damaging than the linear damage rule would suggest. This is similar to the well-known effect in metal fatigue where the linear damage rule is non conservative if the more damaging cycle condition is applied first. Note that 1-hour cycles are more damaging than the 24-hour cycles in terms of survivable hot time.

For the Type II specimens that underwent multi-temperature tests, the linear damage rule is once again reasonably satisfied. Both samples subjected to this loading condition had TBC damage in the range of 0.89 to 0.84, still within reason for the linear damage rule, but the remaining life was over estimated. Multiple hold time tests were not conducted on Type II TBC's.

4.2 Remaining Life Estimates from Stress vs Life Fraction Curves for Type I and II TBC's

In addition to utilizing the linear damage rule on multi-amplitude testing, the remaining life of TBC samples can also be estimated from PLPS measurements taken throughout the duration of the furnace cycling tests and compared to actual life fraction values [10]. In the simple case of single amplitude conditions, reading stress values at the specific test condition will provide a reasonable estimate of remaining life. In discussing non-constant condition testing, we need to pay attention to which cyclic condition is applied first. We will label the first

applied condition as A and the second condition applied as B. For the non-constant tests the success of the life prediction depends on how much information is available. Three different cases were examined.

Case 1: Averaging Multiple History Curves

In this case we assume that all that is known is a single measured stress value and the number of cycles or flight hours at which the measurement is made. To use this limited information for life prediction, the TGO stress versus life fraction for all baseline tests are averaged and used to predict the life for the multiple amplitude tests. In this case, it is assumed that all that is known is the measured stress value at half the expected life and the number of cycles to that point. By averaging baseline 1-hour tests at 1121^{o}C and 1151^{o}C along with the 1-hour 1121^{o}C and 24-hour 1121^{o}C tests a new master curve was generated and compared to the TGO stress versus life fraction curves for the multiple amplitude tests. Various stress values and corresponding life fractions were compared for the new averaged baseline to the two-stage tests for Type I TBC's. This approach was not successful with error ranging from 3% to 91% on predicting remaining life. Insufficient data was available to attempt this approach on Type II samples.

Case 2: Extrapolating Multiple History Curves

Based on observations of the data collected, the stress at failure is relatively constant as is the slope of each curve after the condition change. Accordingly this presents an opportunity to make predictions if two stress measurements are made and the stress is extrapolated to the critical value for failure. To examine this option, we choose to make the two measurements, one at the condition switch of 0.5 life fraction and one at a later time chosen to be at a life fraction of

0.75. In actual cases the measurements would be made at intervals that were convenient and estimated to be at for example 0.5 and 0.75 life fractions. There are clearly many ways to do this and here we somewhat arbitrarily choose to take measurements at life fractions of 0.5 and 0.75 to give a sense of how well or badly this Type of procedure might work. Baseline data is not needed in this approach. The results from this procedure are shown in Table VIII for Type I TBC's. In each case, the number quoted is the predicted life fraction failure divided by the actual one where 1.0 would indicate perfect agreement and numbers larger than 1.0 indicate that the actual life is shorter than the predicted one and hence are anticonservative. The error on total life is also presented as well as the error on the remaining life. The life fraction ratios predicted ranged between 0.87 and 1.045 for a step change in temperature and between 1.34 and 2.38 for a step change in hold time. Not enough testing and information was available to attempt this approach on Type II Samples. As with the linear damage rule, the predictions for a step change in temperature were very good and for a change in cycle durations the predictions were not as good. The stress versus life fraction curves for the two 24-hour tests are not straight with the slope increasing rapidly near the end of the test and as a result linear extrapolation was not very successful.

Case 3: Stress, Life Fraction and the Transition from Condition A to B is Known

The final circumstance for estimating remaining life involves the scenario where the TGO stress, hot time, and cycles after the transition from condition A to B are known. The goal is to use the stress measured at the transition and knowledge of the baseline TGO stress versus life fraction curve slope to determine the remaining life. The main challenge is the fact that there is an offset between the stress level at the transition and the constant condition curve for condition B as seen in Figure 4.1. This offset is the difference in stress at the baseline condition

B compared to the multiple amplitude tests at B. In the cycling conducted, the transition point was chosen to be at a life fraction of approximately 0.5. Table IX shows the size of these offsets for the various tests. The procedure is to extend a stress versus life fraction line known for condition B beginning at the measured value at the transition and predict the life by where that line intersects the critical stress value. This is similar to case 2, but in this case the extrapolation is based on the exact curve from the test data at condition B and not a straight line extrapolation and no second measurement is required. The last column in Table IX shows the predicted failure life fraction divided by the actual one such that numbers greater than 1 are anticonservative predictions where the predicted life exceeded the actual one. In addition, the error on total life prediction is represented as well as the error on the remaining life. The results are reasonable with the largest deviation from a damage of 1.0 is the value of 1.26.

4.3 Premature Failure of Type A Samples

Recall first that all samples of Type A and B were tested using 1 hour cycles at 1121^{o}C. In both Type A samples cycled in furnace testing, premature failure was seen as sample life was less than half of the expected life in similarly deposited thermal barrier coatings [25]. Both samples failed prematurely and with a large standard deviation in furnace cyclic life, suggesting that defects in the processing of the bond coats and TBC's was the cause. Scanning electron microscopy and x-ray diffraction was used to identify the specific damage mechanisms that led to these early failure lives.

4.3.1 SEM Microscopy of Type A Samples

Following the scattered and premature failure of Type A samples, energy-dispersive X-ray spectroscopy (EDX) was utilized in the scanning electron microscope to try and identify the specific bond coat composition and examine the TGO growth and potential failure mechanisms.

For the as-received Type A sample, Figure 4.2 shows the two layered bond coat, and the composition of each layer with the top layer shown as A, and the bottom layer as B. Platinum is more prevalent in the lower bond coat layer with the white shapes spread throughout the bottom bond coat. Aluminum is relatively consistent throughout with nickel, chromium, and cobalt being dispersed evenly in both layers.

Following 220 thermal cycles leading to failure, sample A1 was observed and examined using SEM and EDX scans. The TGO growth in sample A1, although varying in thickness was consistently alpha-alumina with no other elements noted in the TGO as aluminum concentrations were near 70 wt. % in location A shown in Figure 4.3. In addition, high levels of cobalt oxide were found near the bond coat/TGO interface and are designated as B in Figure 4.3. These large structures are spread throughout the sample and in some areas contain no TGO growth above it. These areas give way to cobalt formation on the surface of the bond coat, and thus cause early failure lives as alpha-alumina formation is inconsistent. Cobalt concentrations near the surface reach 55 wt. %.

Sample A3, which failed at 160 cycles, shown in Figure 4.4 was shown to demonstrate similar properties as sample A1 and also failed prematurely during furnace cycling. The TGO growth varied in thickness throughout the sample, but was determined to be alpha-alumina in most locations using elemental scans with aluminum concentrations near 70 wt. % (location A). However, similar to sample A1, cobalt oxide concentrations were extremely high near the surface of the bond coats at the bond coat/TGO interface as shown in location B. Once again, in certain locations, alpha-alumina growth was limited as cobalt formed on the surface of the sample causing failure.

4.3.2 X-Ray Diffraction of Type A Samples

In addition to SEM microscopy of the bond coat, TGO and surface composition in Type A samples, x-ray diffraction of failed samples was utilized to verify the formation of cobalt on the surface. TGO on Type A samples was relatively consistent in terms of growth with varying thickness and in certain regions gave way to large concentrations of cobalt on and near the surface. Following delamination of the ceramic top coat, the exposed Type A samples were scanned for surface composition. Figure 4.5 highlights the x-ray diffraction performed and associated elemental peaks. The peaks at 25^{o} and 35^{o} coincide with alpha-alumina but other peaks shown in blue include cobalt and nickel metal peaks as well. The surface analysis of the Type A samples highlights the formation of cobalt oxide formation on the surface of the samples during thermal cycling. Although largely alpha-alumina TGO, the zones where cobalt reached the surface formed cobalt oxide causing the early failure in observed in Type A samples.

4.4 Premature Failure of Type B Samples

Following the furnace cycling of Type B samples it was noted that sample lives had considerable variability and that the failure was premature for most samples compared to similar samples we have tested. SEM analysis of the bond coat and TGO formation was conducted along with XRD to try and determine why these samples had such early failure lives.

4.4.1 SEM Microscopy of Type B Samples

Firstly, an as-received sample, Type B sample was analyzed in the SEM and EDX scans were performed throughout the sample to determine the specific bond coat composition of the layers to try and understand this newer coating structure. Figure 4.6 shows the two layered bond coat along with the specific compositions in the top layer A, and the bottom layer, B. The top layer in Type B samples contain large concentrations of platinum, around 30-40 wt. %, with less

nickel atoms as well. Chromium and cobalt concentrations are consistent throughout both layers while the lower bond coat contains very little platinum, around 7 wt. %. Lastly, aluminum levels are consistent and steady in both layers.

Following all thermal cycling, sample B2 was examined as it had the longest cyclic life of all samples at 520 1-hour cycles. Due to the long cyclic life of sample B2, the TGO was thick in certain regions, but also varied over the cross-section of the sample due to bond coat rumpling effects with thicker TGO growth on inward displacements. Figure 4.7 shows the bond coat composition at certain points and highlights the cobalt formation near the surface of the TGO, and the platinum rich segregation in the bond coat. The TGO is primarily alpha-alumina with roughly 50 wt. % aluminum and 50 wt. % oxygen. In addition, cobalt oxide formations are prevalent in the bond coat near the surface at the TGO to TBC (now air) interface. In some areas, this grows and reaches the surface as shown in Figure 4.7 and contains nearly 63 wt. % cobalt. Over the course of cycling, depletion of aluminum may have caused this leading to spallation of the ceramic top coat.

In addition to sample B2, sample B5 was examined in the SEM to examine the bond coat composition and TGO growth to try and determine the failure mechanisms that led to spallation at 80 cycles at 1121^{o}C. Figure 4.8 displays sample B5 in cross-section view and highlights the cobalt oxide formation near the surface of the TGO/BC interface. As shown, TGO growth varies greatly and is thicker in certain areas with lighter TGO locations signifying cobalt nickel formation. Similar to sample B2, white cobalt rich grains are scattered throughout and undulations in the bond coat give rise to thick areas of TGO growth throughout the sample. TGO composition in these thick regions contained aluminum levels around 25-30 wt. % with cobalt levels around 15 wt. % as well resulting in a non-homogenous alpha-alumina TGO. In addition,

cobalt oxide formations near the surface contained 75 wt. % cobalt by EDX similar to other samples and are shown as the lighter phase near the surface. This sample, and other premature Type B samples all contained large areas of cobalt nickel oxide formation near the surface, indicating a non-alpha alumina TGO leading to the premature failure seen throughout Type B lives.

4.4.2 X-Ray Diffraction of Type B Samples

X-ray diffraction was performed on the surface of failed Type B samples to obtain an overall surface composition of samples in which the ceramic top coat had spalled off. Figure 4.9 highlights the peaks associated with the TGO/BC interface that had been exposed following furnace cycling failure. Premature failure was noted in the samples at 80 1-hour cycles and heavy cobalt-nickel oxide formation was seen throughout the sample. Unlike Type A samples which contained large areas of alpha-alumina and scattered cobalt nickel oxides on the surface, Type B samples showed minimal alpha-alumina TGO growth. Peaks at 35^{o} and 58^{o} corresponded to α-Al_2O_3 TGO while all other peaks contained cobalt-nickel oxides and zirconium oxide scattered across the surface of the sample. The large cobalt-nickel formation and lack of alpha-alumina had led to the premature failures in Type B samples.

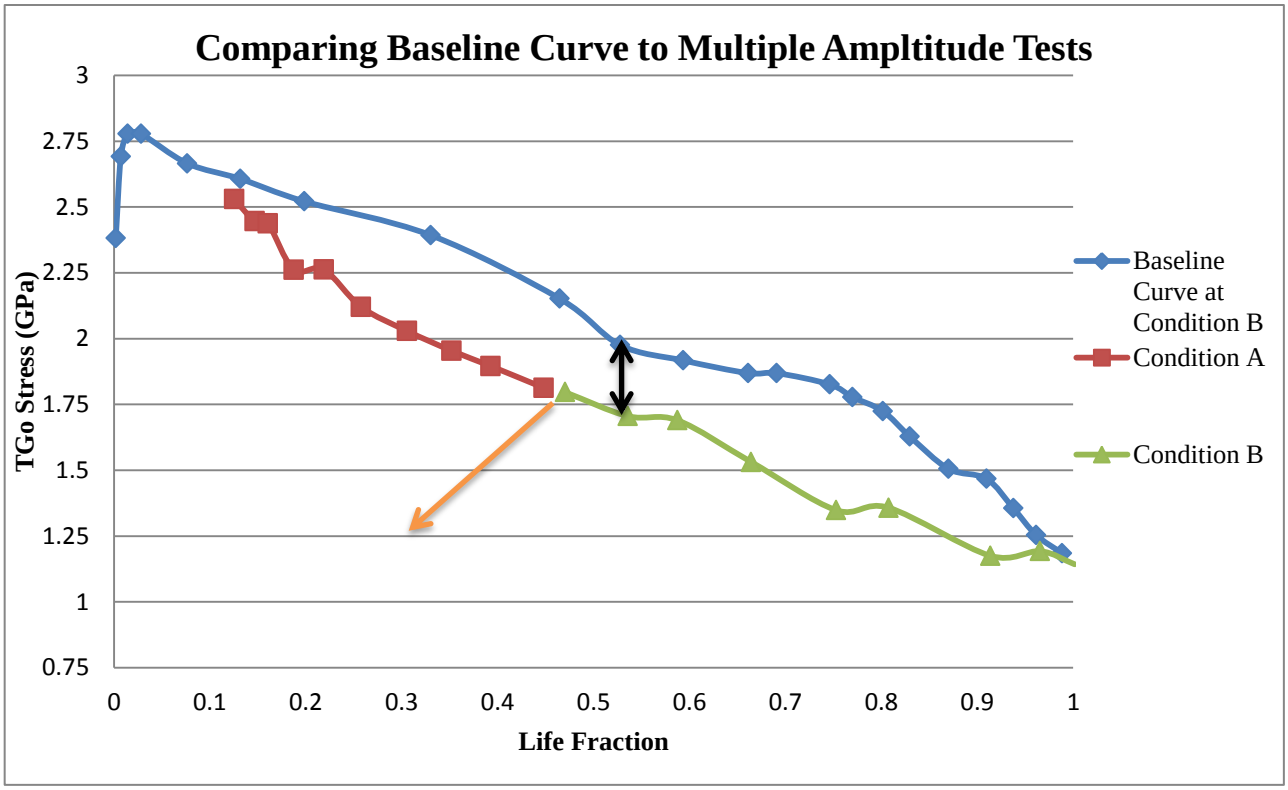

Figure 4.1: Baseline curve at condition B compared to the multiple amplitude tests

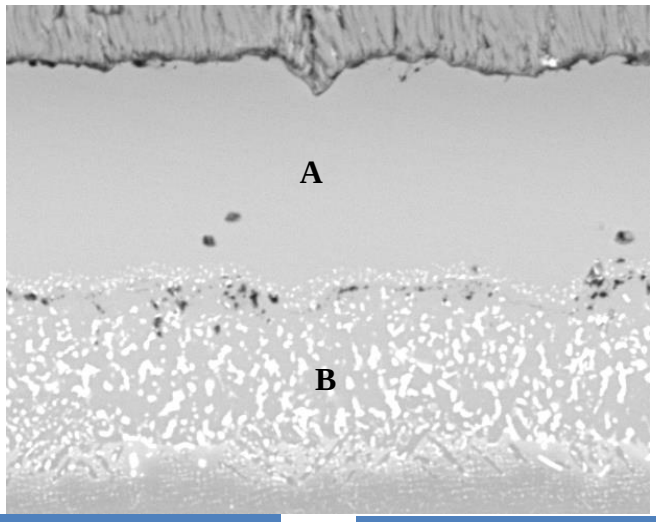

Top Layer Composition (A)	
Element	**Weight %**
Al K	28.31
Cr K	2.68
Co K	4.60
Ni K	36.89
Pt K	27.52

Bottom Layer Composition (B)	
Element	**Weight %**
Al K	23.53
Cr K	4.41
Co K	5.76
Ni K	32.48
Pt K	33.82

Figure 4.2: SEM cross section of as-received Type A sample highlighting the two layered bond coat. The element concentrations of each layer, A and B, are shown in terms of wt. % for the following elements.

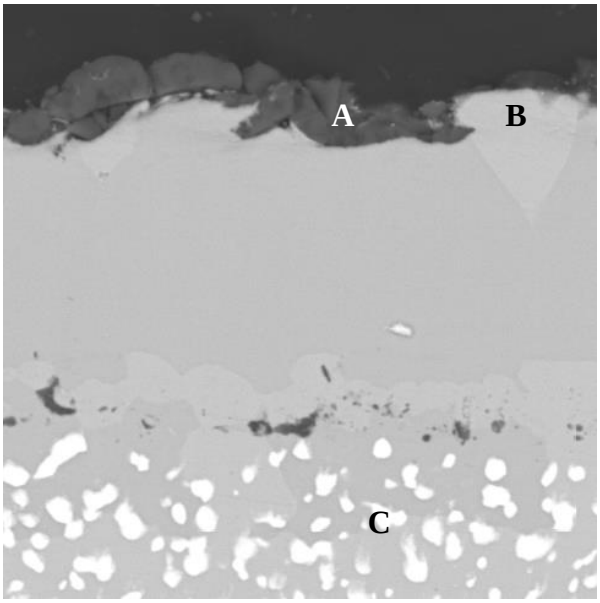

TGO Composition (A)	
Element	**Weight %**
Al K	67.91
O K	32.09

Cobalt Oxide near Surface (B)	
Element	**Weight %**
O K	20.11
Al K	16.95
Pt K	6.2
Co K	55.07
Ni K	1.02

Heavy Elements in lower bond coat (C)	
Element	**Weight %**
Al K	9.02
Cr K	1.54
Co K	28.68
Ni K	1.17
Pt K	59.59

Figure 4.3: SEM cross section of Type A sample A1 with point scans in three locations. Location A is the alpha alumina TGO, while location B is a concentration of cobalt near the surface. Location C shows the platinum and heavier elements segregated in the lower bond coat.

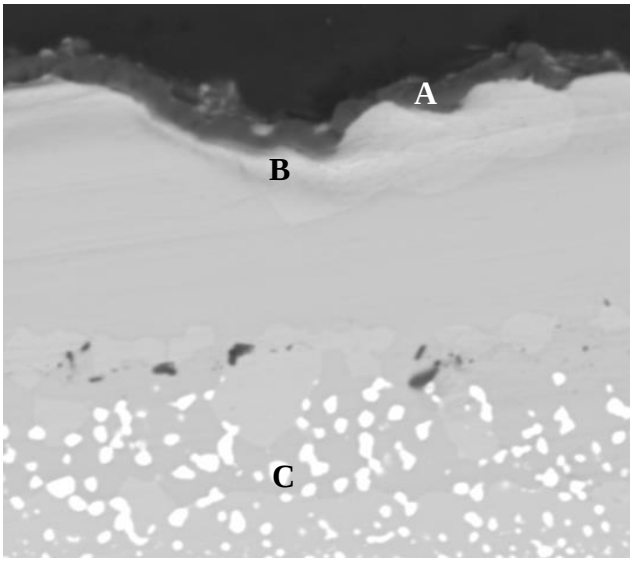

TGO Composition (A)	
Element	**Weight %**
Al K	71.05
O K	25.96
Cr K	0.39
Co K	0.58
Ni K	2.02

Cobalt Oxide near Surface (B)	
Element	**Weight %**
O K	18.63
Al K	13.73
Pt K	0.0
Co K	65.41
Ni K	1.22

Heavy Elements in lower bond coat (C)	
Element	**Weight %**
Al K	9.48
Cr K	1.45
Co K	28.40
Ni K	1.09
Pt K	59.57

Figure 4.4: SEM cross section of Type A sample A3 with point scans in three locations. Location A designates the TGO, while location B is a concentration of cobalt near the surface. Location C shows the platinum and cobalt concentrations in the lower bond coat.

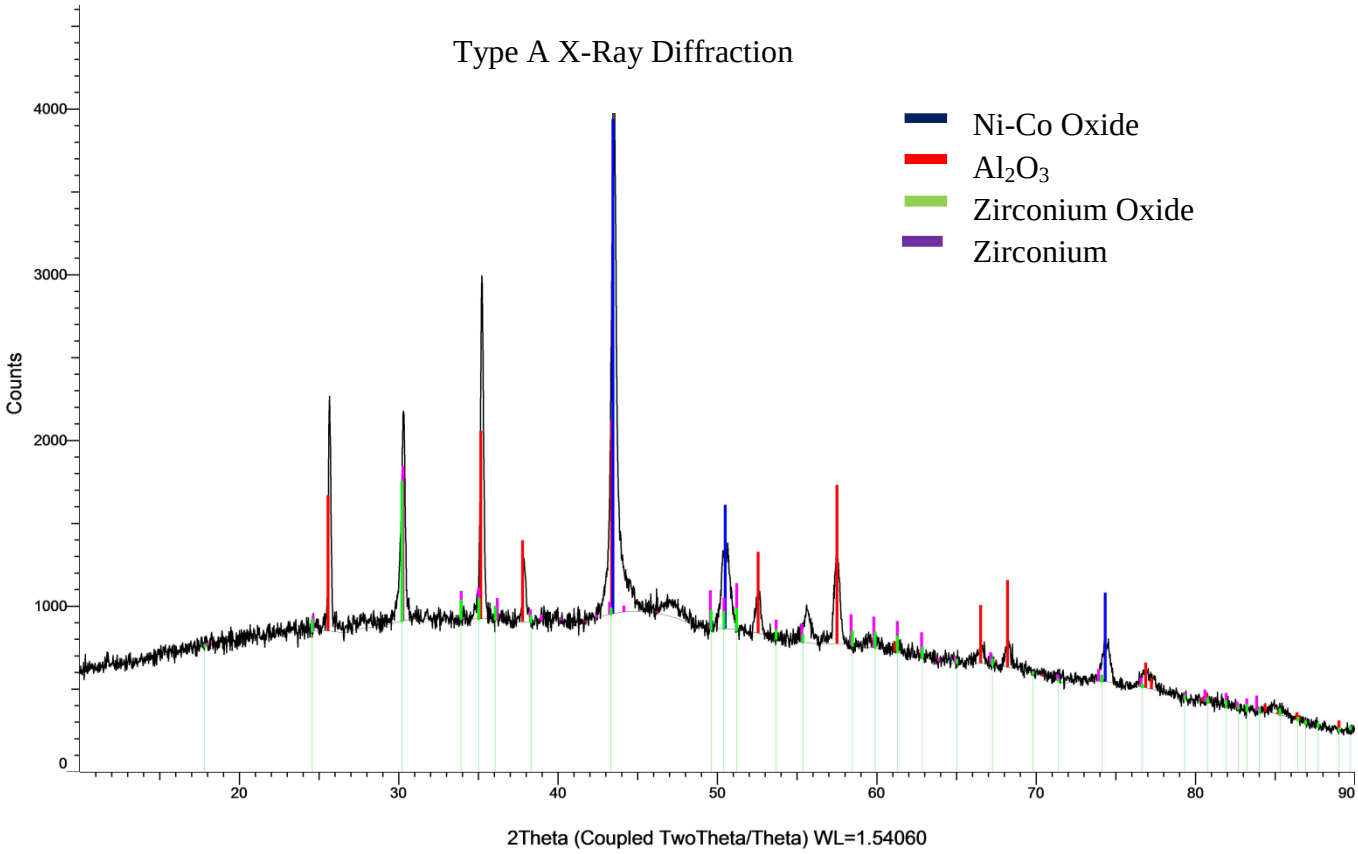

Figure 4.5: X-Ray diffraction on spalled Type A sample. Peaks are highlighted by the corresponding elements with most peaks belonging to alpha-alumina oxide. The largest peak was for nickel-cobalt oxide shown in blue.

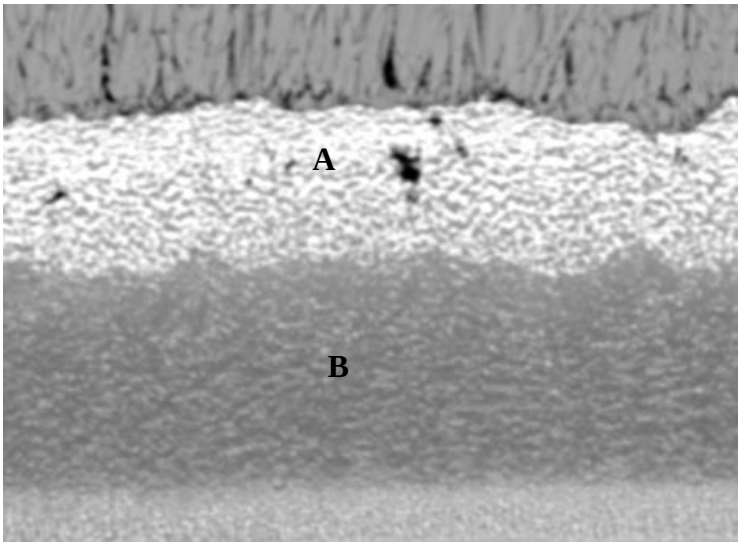

Top Layer Composition (A)	
Element	**Weight %**
Al K	34.99
Cr K	3.54
Co K	3.19
Ni K	20.40
Pt K	37.89

Bottom Layer Composition (B)	
Element	**Weight %**
Al K	43.22
Cr K	4.69
Co K	6.42
Ni K	38.14
Pt K	7.54

Figure 4.6: SEM composition scans on as-received Type B sample. Top layer, A, shows larger platinum concentration, while the lower bond coat layer, B has platinum levels around 7%.

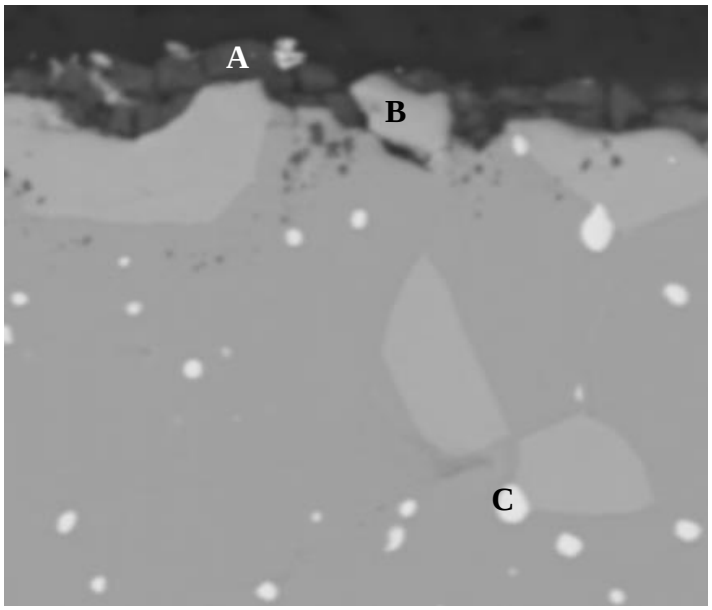

TGO Composition (A)	
Element	**Weight %**
Al K	48.27
O K	48.94
Cr K	0.16
Co K	0.28
Ni K	0.35

Cobalt Oxide near Surface (B)	
Element	**Weight %**
O K	17.79
Al K	14.9
Pt K	0.57
Co K	63.91
Ni K	2.06

Heavy Elements in lower bond coat (C)	
Element	**Weight %**
Al K	12.54
Cr K	1.17
Co K	56.38
Ni K	0.57
Pt K	29.34

Figure 4.7: SEM cross-section view of Type B sample B2 post furnace cycling. Location A shows the TGO and the corresponding element composition highlighting alpha-alumina formation. Location B designates the cobalt oxide formation at the surface with no TGO growth above it while location C is a platinum rich grit in the bond coat.

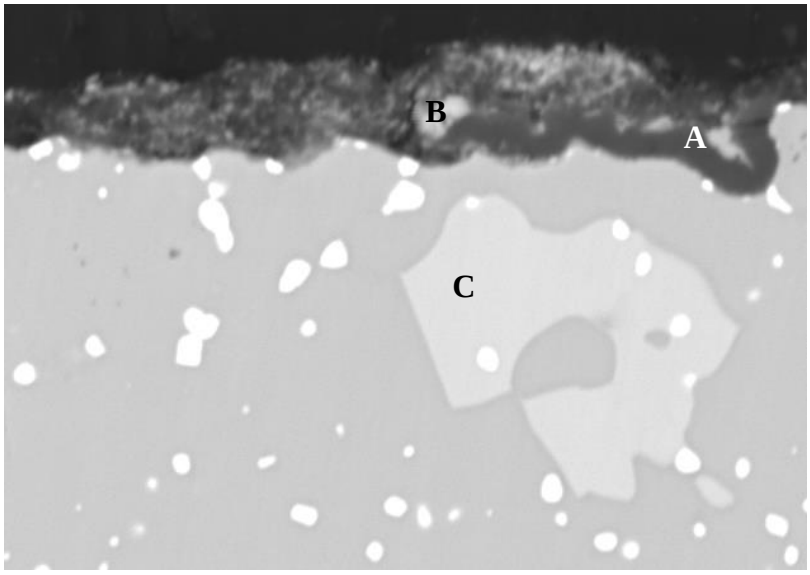

TGO Composition (A)	
Element	**Weight %**
Al K	27.34
O K	56.18
Cr K	0.32
Co K	16.16
Ni K	0.0

Cobalt Oxide near Surface (B)	
Element	**Weight %**
O K	13.27
Al K	2.43
Pt K	5.73
Co K	75.71
Ni K	2.32

Heavy Elements in lower bond coat (C)	
Element	**Weight %**
Al K	14.30
Cr K	0.45
Co K	72.41
Ni K	0.83
Pt K	0.68

Figure 4.8: Cross-section of Type B sample B5 highlighting the light colored cobalt oxide formation on the surface of the TBC/BC interface. The non-uniform alpha-alumina TGO formation is shown throughout the sample. Heavy elements are segregated in the bond coat layer as well.

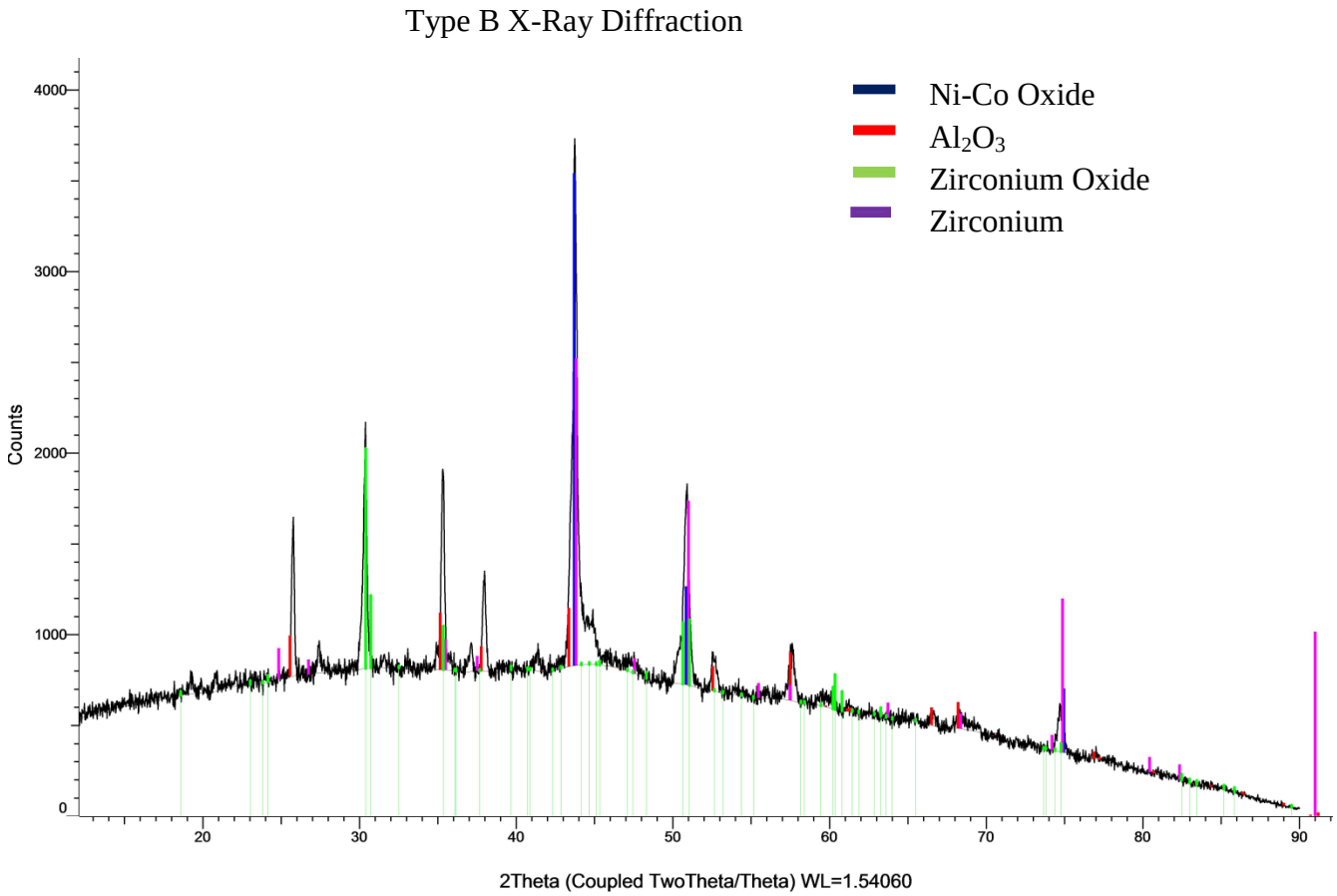

Figure 4.9: X-Ray diffraction on spalled Type B sample. Peaks are highlighted by the corresponding elements with most peaks belonging to cobalt-nickel oxide. The largest peak was for nickel-cobalt oxide shown in blue with few peaks for alpha-alumina.

Table VI: Linear Damage Coefficients for Type I TBC's [25]

Sample	**Test Condition A**	**Damage Fraction at A**	**Test Condition B**	**Damage Fraction at B**	**Total TBC Damage**	**Percent Error (%)**
LD 73	1121^{o}C 1-Hour	0.494	1151^{o}C 1-Hour	0.573	1.067	6.7
LD 74	1121^{o}C 1-Hour	0.494	1151^{o}C 1-Hour	0.628	1.122	12.2
LD 82	1151^{o}C 1-Hour	0.5167	1121^{o}C 1-Hour	0.5022	1.018	1.8
LD 84	1151^{o}C 1-Hour	0.5167	1121^{o}C 1-Hour	0.604	1.121	12.1
LE 33	1121^{o}C 1-Hour	0.509	1121^{o}C 24-Hour	0.244	0.753	24.7
LE 04	1121^{o}C 24-Hour	0.488	1121^{o}C 1-Hour	0.4401	0.928	7.2

Table VII: Linear Damage Coefficients for Type II TBC's [25]

Sample	**Test Condition A**	**Damage Fraction at A**	**Test Condition B**	**Damage Fraction at B**	**Total TBC Damage**	**Percent Erorr (%)**
LV 37	1121^{o}C 1-Hour	0.4635	1151^{o}C 1-Hour	0.4325	0.89	11
LV 48	1151^{o}C 1-Hour	0.4545	1121^{o}C 1-Hour	0.387	0.841	15.9

Table VIII: Total life fractions for multiple amplitude tests for Type I TBC's and error on total and predicted life

Type I TBC	$\frac{\textbf{\textit{Predicted Life Fraction}}}{\textbf{\textit{Actual Failure Life Fraction}}}$	**Total Life Error (Remaining Life Error)**
1121^{o}C to 1151^{o}C (1-Hour)	1.045	4.5% (14.52%)
1151^{o}C to 1121^{o}C (1-Hour	0.87	13% (24%)
1 hour to 24 hour (1121^{o}C)	1.34	34% (103%)
24 hour to 1 hour (1121^{o}C)	2.38	138% (151.3%)

Table IX: Stress offset, total life fractions, and error for multiple amplitude tests

Type I TBC	**Offset between baseline and condition B (GPa)**	$\frac{\textbf{\textit{Predicted Life Fraction}}}{\textbf{\textit{Actual Failure Life Fraction}}}$	**Total Life Error (Remaining Life Error)**
1121^{o}C to 1151^{o}C (1-Hour)	-0.13	1.01	1% (3.2%)
1151^{o}C to 1121^{o}C (1-Hour	0.25	1.16	16% (29.5%)
1 hour to 24 hour (1121^{o}C)	0.34	1.05	5% (15.15%)
24 hour to 1 hour (1121^{o}C)	-0.30	1.02	2% (2.2%)
Type II TBC	**Offset between baseline and condition B (GPa)**	$\frac{\textbf{\textit{Predicted Life Fraction}}}{\textbf{\textit{Actual Failure Life Fraction}}}$	**Total Life Error (Remaining Life Error)**
1121^{o}C to 1151^{o}C (1-Hour)	-0.53	0.99	1% (2.8%)
1151^{o}C to 1121^{o}C (1-Hour)	0.59	1.26	26% (46.4%)

5. Conclusion

Life Prediction of Thermal Barrier Coatings

The linear damage rule was shown to do a reasonable job at remaining life prediction for samples undergoing a change in temperature during cycling with a maximum error of 16% and less well for tests samples undergoing multiple hold times with a maximum error of 24%. These conclusions held for the two Types of samples tested here. The use of measured TGO stress to predict remaining life followed the same pattern, working reasonably well when cycle temperature was suddenly changed part way through the test but not nearly as well if the cycle hold time was suddenly changed.

Overall, the non-destructive evaluation technique using PLPS to measure TGO stress is useful in life prediction of EB-PVD thermal barrier coatings for constant and non-constant tests. However, it was shown that in the case of a step change in conditions, it is not possible to estimate remaining to a useful accuracy from a single stress measurement and no other information. The measured stress at failure is nearly a constant. If two measurements of stress are made the rate of change of stress with time or cycles can be estimated and the time to reach the critical stress can be predicted. For Type I samples involving sudden temperature change the life can be estimated to a life fraction that at worst is off by 13% while for a sudden change in cycle duration the estimate is at worst 138%. The worst estimate is for the case cycling for 24 hours at 1121^{o}C then changing the hold time to 1-hour to failure.

If the temperature and cycle duration are known for the remainder of the test a single measurement of stress can be combined with the slope and curve shape known from base line testing at the know conditions can be used to predict when the stress reaches the critical TGO

stress level . The resulting in maximum errors for temperature change was 16% for Type I TBC's, 26% for Type II TBC's and for change in cycle duration was 5%. Since stress measurement may require opening the engine case, reducing the measurement need to a single measurement is an important difference. The tests run are in a way the worst case since only two conditions were used and any sequence effects would not average out. An important question yet to be answered is what sort of accuracy can be expected from a linear damage rule or from PLPS measurements for multilevel tests or random load level tests. In analogue with traditional fatigue testing, improved accuracy may be possible. Such experiments are encouraged.

Type A and Type B TBC Life Prediction

In the case of the two newer coating systems experimentally tested, the life prediction methods discussed previously were not utilized as the samples experienced premature failure lives in furnace cycling. Type A samples, although showing a monotonic decrease in TGO stress during furnace cycling similar to Type I and Type II TBC's, had and average failure life of 190 cycles. TGO growth in Type A samples was generally uniform, and consisted of alpha-alumina but had small areas of cobalt-nickel formation leading to the early failure. Even with the low durability in furnace testing, Type A samples showed TGO stress data that was encouraging indicating that these samples could be examined using the life prediction methods generated.

For Type B samples, the large scatter of failure lives and growth of non-uniform alpha and other oxides indicate that these samples could not be studied using the TGO stress life prediction models. Type B samples experienced very little decay in stress during cycling and the lack of uniform TGO growth highlights the issues with bond coat processing on these samples. Without proper alpha-oxide formation and stress decay during cycling, the PLPS measurement to

predict remaining life of these samples does not look promising. The top layer of the bond coat contained higher platinum concentrations and showed a distinct two layer bond coat that may have not been deposited and treated correctly. The Type B samples had almost no initial TGO layer in the as-received condition indicating improper heat treatment during processing leading to the lack of alpha-alumina growth. The absence of a TGO layer was notable in both SEM cross sections and in absence of any PLPS signal . In past experiments PLPS could detect TGO even when it was not seen in the SEM. Absent an initial layer of alpha alumina these samples will undergo transient oxidation during which non alpha oxides would be expected for form. In most bond coats eventually alpha alumina will dominate after a transient period. This did not happen in Type B samples. It is worth noting that these samples had a two layer bond coat that was very platinum rich in the surface layer and it is likely this composition was not conductive for the formation of alpha alumina to dominate over the time that it took these samples to fail. Change in the processing to correct this composition problem and the absence of initial alpha alumina layer is recommended.

References

[1] David R. Clarke, Simon R. Phillpot, Thermal barrier coating materials, Materials Today, Volume 8, Issue 6, June 2005, Pages 22-29, ISSN 1369-7021, http://dx.doi.org/10.1016/S1369-7021(05)70934-2.

[2] Nicholls J. R., Rickerby D. S., Materials and Processes for High Temperature Surface Engineering", Proc. Materials Congress 1998 in Cirenchester, in "B278-Materials for High Temperature Power Generation and Process Plant Application", Ed. A. Strang, IOM Communications Ltd. 279 (2002).

[3] R. L. Jones, "Thermal Barrier Coatings"; pp. 194–235 in Metallurgical and Ceramic Coatings. Edited by K. H. Stern. Chapman and Hall, London, U.K., 1996.

[4] N.P. Padture, M. Gell and E.H. Jordan, "Thermal Barrier Coatings for Gas-Turbine Engine Applications," ***Science***, **296**, 280-284 (2002).

[5**]** X.Q. Cao, R. Vassen, D. Stoever, Ceramic materials for thermal barrier coatings, Journal of the European Ceramic Society, Volume 24, Issue 1, January 2004, Pages 1-10, ISSN 0955-2219, http://dx.doi.org/10.1016/S0955-2219(03)00129-8.

[6] Schulz U., Oettel, H., Bunk, W., Zeitschrift fuer Metallkunde 87 488-492 (1996).

[7] Stecura S., NASA-TM-86905 (1985).

[8] Morrel P., Rickerby D. S., In: AGARD-R-823 20 (1998).

[9] Terry, S.: "Microstructural evolution of thermal barrier coatings grown by physical vapor

[10] Lipkin D. M., Clarke D. R., Hollatz M., Bobeth M., Pompe W., Corrosion Science 39-2 243 (1997 b).

[11] Chen J. H., Surface & Coatings Technology 92 69-77 (1997)

[12] [5] N.E. Paton, K.S. Murphy, D.R. Clarke, US Patent #6,072,568, 2000.

[13] Lipkin D. M., Clarke D. R., Journal of Applied Physics 77 [5] 1855-1863 (1995).

[14] Christensen R. J., Lipkin D. M., Clarke D. R., Murphy K. S., Applied Physics Letters 69 [24] 3754-3756 (1996).

[15] Lipkin D. M., Clarke D. R., Oxidation of Metals 45 267 (1996).

[16] Clarke D. R., Christensen R. J., Tolpygo V. K., Surface & Coatings Technology 94-95 89-93 (1997).

[17] He J., Clarke D. R., Journal of American Ceramic Society 78 5 1347 (1995).

[18] Selcuk A., Atkinson A., Acta Materialia 51-2 535-549 (2003).

[19] Xie L. D., Sohn Y. H., Jordan E. H., Gell M., Surface & Coatings Technology 176-1 57-66 (2003).

[20] Swetha Sridharan, Liengde Xie and Eric H. Jordan and Maurice Gell, "Stress Variation with Thermal Cycling in the Thermally Grown Oxide of an EB-PVD Thermal Barrier Coating, Surface Coatings and Technology,Vol 179, issues 2-3, Feb,2004, pp. 286-298.

[21] Mei Wen, Eric H. Jordan and M. Gell. Evolution of Photo-stimulated Luminescence of EB-PVD Thermal Barrier Coatings, Materials Science and Engineering A, 398 (2005), 99-107.

[22] Ahmadian, S., Thistle, C., Jordan, E. H. (2013), Experimental and Finite Element Study of an Air Plasma Sprayed Thermal Barrier Coating under Fixed Cycle Duration at Various Temperatures. Journal of the American Ceramic Society, 96: 3210–3217.
doi: 10.1111/jace.12552

[23] Hawron, Martin P., "Non-Destructive Evaluation and Maintenance of Thermal Barrier Coatings" (2014). *Master's Theses.* Paper 648.
http://digitalcommons.uconn.edu/gs_theses/648

[24] Pennefather R. C., Boone D. H., Surface & Coatings Technology 76–77 47 (1994).

[25] Sridharan, Swetha, "Thermal cycle parameter effects on the stress state, failure mechanisms and life prediction of thermal barrier coatings" (2005). *Doctoral Dissertations.* Paper AAI3193744.

http://digitalcommons.uconn.edu/dissertations/AAI3193744

Appendix

PLPS stress and life fraction values extracted from [25] for constant amplitude tests

Type I: 1121°C 1-Hour	
Life Fraction	**Average TGO Stress**
0.001755926	2.3823528
0.007023705	2.6925135
0.01404741	2.778075
0.02809482	2.778075
0.07638279	2.6657753
0.13169447	2.606952
0.19841966	2.5213904
0.33011413	2.393048
0.4644425	2.1524065
0.52765584	1.9759358
0.59350306	1.9171124
0.6611062	1.868984
0.69095695	1.868984
0.74626863	1.8262032
0.76997364	1.7780749
0.8015803	1.7245989
0.82967514	1.6283423
0.87006146	1.5053476
0.9095698	1.4679145
0.9376646	1.355615
0.96136963	1.2540107
0.9885865	1.184492

Type I: 1151°C 1-Hour	
Life Fraction	**Average TGO Stress**
0.01310616	2.658177
0.05067715	2.8458445
0.08562691	2.899464
0.09785933	2.7707775
0.12581913	2.7707775
0.15640017	2.6689007
0.18698122	2.647453
0.2105723	2.6152816
0.23940586	2.577748
0.26299694	2.5563002
0.28309307	2.4919572
0.3119266	2.4865952
0.3634775	2.4544237
0.41415465	2.3686328
0.46395805	2.3096514
0.49890783	2.27748
0.5399738	2.1809652
0.5714286	2.1541555
0.62647444	2.100536
0.6972477	1.961126
0.7470511	1.7841823
0.7741372	1.7091153
0.8125819	1.6018766
0.88248146	1.4785522
0.9156837	1.3552278
0.99781567	1.1139411

Type I: 1121°C 1-Hour	
Life Fraction	**Average TGO Stress**
0.10135638	2.6493318
0.13316213	2.560833
0.1496463	2.5315287
0.1990573	2.5331676
0.21911697	2.4044776
0.33213022	2.2490196
0.37450558	2.200673
0.46280873	2.0543458
0.5228678	1.9269828
0.5899394	1.8993561
0.6558207	1.9015414
0.67700154	1.8922935
0.7393812	1.83466
0.7617661	1.7657497
0.790024	1.7169349
0.82184815	1.5886352
0.8406991	1.5295581
0.87483466	1.4908887
0.89719653	1.4717296
0.91603357	1.4425032
0.94427305	1.4334894
0.96079415	1.3245829

Type I: 1121°C 24-Hour	
Life Fraction	**Average TGO Stress**
0.10235294	2.680921
0.14470588	2.631579
0.19294117	2.6611843
0.21411765	2.5921052
0.29294118	2.5032895
0.30941176	2.5230262
0.3635294	2.4835527
0.4117647	2.4539473
0.4364706	2.3848684
0.48705882	2.4243422
0.50941175	2.3947368
0.58235294	2.305921
0.6141176	2.3256578
0.6552941	2.3256578
0.7223529	2.2664473
0.7776471	2.3157895
0.81529415	2.256579
0.8364706	2.2072368
0.8729412	2.1578948
0.90705884	2.1282895
0.9211765	2.1776316
0.9823529	1.8125
0.9988235	1.4375

Type II - 1121°C 1-Hour	
Life Fraction	**Average TGO Stress**
0.103314854	2.9566898
0.12794456	2.9093294
0.27832347	2.6484983
0.34314698	2.5534132
0.50003785	2.3859982
0.6076727	2.325
0.684139	2.124378
0.8358385	1.9453883
0.94212246	1.6972846
1.0017074	1.4268811

Type II - 1151°C 1-Hour	
Life Fraction	**Average TGO Stress**
0.09925561	2.3719811
0.12133839	2.4884253
0.2794859	2.180628
0.35856977	2.0618174
0.4610233	2.0243325
0.5426877	1.8586771
0.71387595	1.7961924
0.8382979	1.4774879
0.9251739	1.3935832
0.95500845	1.3043
1.0054808	1.0174302

PLPS stress and life fraction values extracted from [25] for multiple amplitude tests

Type I - 1121°C to 1151°C	
Life Fraction	**Average TGO Stress**
0.15385884	2.916934
0.38587722	2.526314
0.40066725	2.5013804
0.4949496	2.3602858
0.51435786	2.3438416
0.5494915	2.252062
0.56797194	2.252407
0.5957096	2.1772957
0.61604184	2.160869
0.67796457	2.1032026
0.7038447	2.070073
0.75285953	1.8861166
0.7695128	1.7939918
0.79538536	1.794475
0.82313067	1.6857507
0.85269934	1.6863029
0.8748967	1.5942817
0.9072469	1.5528696
0.9627204	1.4110502
1.0006337	1.2857094

Type I - 1151°C to 1121°C	
Life Fraction	**Average TGO Stress**
0.12530147	2.5298512
0.14657292	2.4462159
0.16043513	2.4380715
0.18727158	2.2621045
0.21868828	2.262691
0.2575294	2.1205611
0.30559936	2.029023
0.35181746	1.9542568
0.39248767	1.8961935
0.4479479	1.8131967
0.47012818	1.7968043
0.5357545	1.7055941
0.5875035	1.6897539
0.66423327	1.531525
0.752981	1.3483107
0.8074963	1.3577319
0.9138004	1.1748456
0.9655418	1.1926183
1.00159	1.142872

Type I: 1 hour to 24 (1121°C)	
Life Fraction	**Average TGO Stress**
0.08507882	2.6640866
0.2978124	2.5663605
0.6738878	1.9364147
0.8404581	1.7893957
0.96986	1.6942044
0.98022336	1.6127737
0.99622667	1.0546173

Type 1: 24 hour to 1-hour (1121°C)	
Life Fraction	**Average TGO Stress**
0.07599379	2.603217
0.07932213	2.6415334
0.08819853	2.7411594
0.10662345	2.584553
0.29651242	2.514755
0.8467103	2.247665
0.99951637	1.4923469

Type II- 1121°C to 1151°C	
Life Fraction	**Average TGO Stress**
0.12048193	2.9692307
0.28674698	2.7769232
0.41807228	2.6153846
0.5373494	2.5384614
0.6253012	2.4692307
0.68192774	2.4230769
0.76626503	2.3307693
0.8879518	2.0846155
0.99879515	1.5307692

Type II - 1151°C to 1121°C	
Life Fraction	**Average TGO Stress**
0.11047395	2.5063186
0.2619966	2.326585
0.36051524	2.0484507
0.42902386	1.9012781
0.44342935	1.8396425
0.61776793	1.5750912
0.7380468	1.4727067
0.87035495	1.3623824
0.86862797	1.3669062
0.9995022	1.1653941